THE GEOLOGICAL SOCIETY OF AMERICA®

Clockwise rotations recorded in redbeds from the Jinggu Basin of northwestern Indochina

Shihu Li[1,†], Zhenyu Yang[2], Chenglong Deng[1], Huaiyu He[3], Huafeng Qin[1], Lu Sun[1], Jie Yuan[1,4], Douwe J.J. van Hinsbergen[5], Wout Krijgsman[6], Mark J. Dekkers[6], Yongxin Pan[3], and Rixiang Zhu[1]

[1]*State Key Laboratory of Lithospheric Evolution, Institute of Geology and Geophysics, Chinese Academy of Sciences, Beijing 100029, China*

[2]*College of Resources, Environment and Tourism, Capital Normal University, Beijing 100048, China*

[3]*CAS Key Laboratory of Earth and Planetary Physics, Institute of Geology and Geophysics, Chinese Academy of Sciences (CAS), Beijing 100029, China*

[4]*University of Chinese Academy of Sciences, Beijing 100049, China*

[5]*Department of Earth Sciences, University of Utrecht, 3584 CD Utrecht, The Netherlands*

[6]*Paleomagnetic Laboratory "Fort Hoofddijk," Department of Earth Sciences, Utrecht University, Budapestlaan 17, 3584 CD, Utrecht, The Netherlands*

ABSTRACT

Paleomagnetic data have been used to infer clockwise rotations and significant southward motion of the Indochina block during Cenozoic extrusion from the India-Asia collision zone. Because the Cenozoic of the Indochina block has been sparsely sampled to date and is key to determining the timing of this tectonic motion, we performed an extensive paleomagnetic study on Paleocene to Oligocene redbeds and middle Miocene sandy silts from the Jinggu Basin (23.5°N, 100.7°E), in northern Indochina. Paleomagnetic results from the redbeds pass fold tests, but they show exclusively normal polarity. There is controversy, however, on the age assignment to the lower part of the succession. If the age of the redbeds is indeed Paleogene, this indicates a prefolding remagnetization associated with Oligocene deformation of the Indochina block. If the age of the redbeds would be Late Cretaceous, their magnetization may be primary, and deposition could have taken place during the Cretaceous normal superchron. However, the abundance of secondary hematite in the redbeds in combination with the biostratigraphy, which indicates a Paleogene age for at least the upper two formations of the redbeds in the Jinggu Basin, implies a pervasive remagnetization. The middle Miocene sediments pass both the fold test and the reversals test and contain magnetite as well as hematite as carriers, suggesting a primary magnetization. Our large data set from the redbeds (>2000 paleomagnetic directions) demonstrates an ~30°–35° clockwise rotation of the Jinggu Basin with respect to Eurasia, for both scenarios, i.e., when compared to a ca. 100 Ma pole (if the redbeds carry a primary natural remanent magnetization) or to a ca. 30 Ma pole (if the sequence is remagnetized). The middle Miocene results, however, indicate that the Jinggu Basin experienced no significant (2° ± 5.6°) rotation with respect to Eurasia. Since no major deformation has occurred within northern Indochina during Late Cretaceous to Eocene times, our results reflect a major clockwise rotation of the Indochina block during its Oligocene to early Miocene extrusion from the India-Asia collision zone.

INTRODUCTION

The early Cenozoic collision of continental crust belonging to the Indian and Eurasian plates led to the formation of the Himalaya orogenic belt, and major shortening in the Tibetan Plateau and in Asia farther to the north (Molnar and Tapponnier, 1975). It also led to the extrusion of the Indochina block along the Ailao Shan–Red River fault in the east and the Shan scarp–Sagaing fault in the west (e.g., Tapponnier et al., 1982; Bertrand et al., 2001). Geological and paleomagnetic studies have indicated that more than 3000–4000 km of plate convergence has occurred since the beginning of collision (van Hinsbergen et al., 2011a, 2012; Lippert et al., 2014), with a ca. 59–50 Ma initial continent-continent collision age (e.g., Dupont-Nivet et al., 2010a; Yi et al., 2011; Hu et al., 2015).

A key element in the discussion of the distribution of crustal shortening accommodating the convergence history of the India-Asia collision is how far the Indochina block was extruded out of Tibet and whether the Indochina block experienced a large-scale clockwise rotation. Since the 1980s, some researchers have proposed that Indochina may have been extruded over as much as 600–1200 km along the Ailao Shan–Red River fault as a quasi-rigid block, associated with as much as 25°–40° clockwise rotation (Tapponnier et al., 1982; Royden et al., 2008), whereas others have suggested a much smaller distance of no more than ~250 km and a moderate rotation of less than 15° (Searle et al., 2010; van Hinsbergen et al., 2011b).

Over the past decades, large numbers of paleomagnetic studies have been conducted on rocks from the Indochina Peninsula and the eastern Tibetan Plateau margin region to constrain its rotation and paleolatitudinal motion history (e.g., Otofuji et al., 1990, 2010; 2012; Huang and Opdyke, 1993, 2015; Yang and Besse, 1993; Yang et al., 1995, 2001; Yang and Otofuji, 2001; Sato et al., 2007; Zhu et al., 2008; Li et al., 2013; Chi and Geissman, 2013; Tong et al., 2013, 2015; Kornfeld et al., 2014a, 2014b; Gao et al., 2015). The paleomagnetic declinations obtained to date suggest that the rotation in the SE margin of the Tibetan Plateau ranges from ~120° clockwise rotation to no significant rotation (e.g., Yang and Besse, 1993; Chen et al., 1995; Yang et al., 1995; Li et al., 2012; Chi and Geissman, 2013; Tong et al., 2013), while the suggested latitudinal displacement based on recovered inclinations varies from 1500 km southward motion to even

†lsh917@mail.iggcas.ac.cn

GSA Bulletin; September/October 2017; v. 129; no. 9/10; p. 1100–1122; doi: 10.1130/B31637.1; 11 figures; 4 tables; Data Repository item 2017144; published online 11 May 2017.

northward motion (see review in van Hinsbergen et al., 2011b), which hampers a proper analysis of the Cenozoic geodynamic evolution of the Tibetan Plateau. However, a rigorous reassessment of the quality and reliability of these data is required, mainly because most of the previous paleomagnetic data have been derived from Mesozoic rock formations, which record the rotation and translation accumulated since pre-Cenozoic times, and therefore cannot exclusively resolve the Cenozoic movements of the India-Asia collision and the formation of Tibetan Plateau (Kornfeld et al., 2014b). Another important factor is the increasing body of evidence showing that remagnetization may have occurred in this area in the Cenozoic (Liu et al., 2011; Yamashita et al., 2011; Kornfeld et al., 2014a; Huang and Opdyke, 2015; Tsuchiyama et al., 2016). Therefore, we collected a large data set of paleomagnetic samples from a Paleogene to Miocene clastic stratigraphic section in the Jinggu Basin, western Yunnan Province, in the northern part of the Indochina block (Fig. 1A).

The Jinggu Basin preserves a nearly continuous stratigraphic section from the Jurassic to Quaternary with a thickness of more than 10 km (Yunnan Bureau of Geology and Mineral Resources [YBGMR], 1990). These sediments thus provide an ideal archive in which to determine the detailed rotation history during the Cenozoic. Chen et al. (1995) conducted a paleomagnetic study on the Lower Cretaceous to Pliocene sediments in the Jinggu Basin (Fig. 1B). However, in that study, no significant paleomagnetic results were isolated from the sampled Eocene and Pliocene sediments. Only the results from the Lower Cretaceous Mangang Formation passed the fold test, taken as an indication by Chen et al. (1995) for a primary characteristic remanent magnetization (ChRM). The in situ directions of the Lower Cretaceous Jingxing Formation and the Paleocene Mengyejing Formation were similar to the tilt-corrected results from the Eocene to Oligocene Denghei and Miocene Sanhaogou Formations and were thus regarded as remagnetized during the Eocene to Oligocene or Miocene (Chen et al., 1995). The reliability of the results from the Eocene–Oligocene Mengla Group, which have both normal and reversed polarity (but only five samples) that seems to be primary, is ambiguous as well because fold and reversal tests are lacking (Chen et al., 1995). Since their results are based on only a limited number of samples (~30 samples for each formation), and no detailed rock magnetic information was provided, the reliability of the paleomagnetic results presented by Chen et al. (1995) is subject to discussion, and whether or not Cenozoic remagnetization occurred in Jinggu Basin remains unknown. In this paper, we present more robust paleomagnetic data from Cenozoic sediments of the Jinggu Basin in an attempt to constrain the temporal distribution of rotation of the Indochina block during the Cenozoic, while carefully testing for pervasive remagnetization.

GEOLOGICAL SETTING AND SAMPLING

Geological Setting

The SE margin of the Tibetan Plateau is composed of a collage of continental blocks, which includes the West Burma, Sibumasu, Indochina, and South China blocks from west to east (Fig. 1A). A striking geological feature in the SE margin of the Tibetan Plateau is the occurrence of large-scale strike-slip faults, such as the Ailao Shan–Red River fault, the Sagaing fault, and the Xianshuihe-Xiaojiang fault (Fig. 1A).

The Ailao Shan–Red River fault is regarded as the eastern boundary of the southeastward extrusion of the Indochina block; its left-lateral ductile shear forms the basis of the extrusion (Tapponnier et al., 1982; Leloup et al., 1995). However, the timing and the amount of displacement along the left-lateral Ailao Shan–Red River fault shear zone have been strongly debated over the last decades. One school argues that the amount of sinistral offset along the Ailao Shan–Red River fault shear zone is 700 ± 200 km and that the slip occurred from the Oligocene to mid-Miocene (35–17 Ma), based on observations along the northwestern part of the Ailao Shan–Red River fault shear zone (Leloup et al., 1995, 2001; Gilley, 2003). They also propose that the activity of the Ailao Shan–Red River fault shear zone was kinematically linked to the opening of the South China Sea (Briais et al., 1993). The other school, however, argues that the displacement of the Ailao Shan–Red River fault shear zone is only 250 km, based on observations along the eastern margin of the Indochina block and offshore (Hall et al., 2008; Searle et al., 2010; van Hinsbergen et al., 2011b), and that the zone was active from 32 to 22 Ma (Searle et al., 2010).

The left-lateral Xianshuihe-Xiaojiang fault is regarded as a boundary fault to accommodate the differential rotations around the eastern Himalayan syntaxis (Schoenbohm et al., 2006; Wang et al., 1998). Its activity started at ca. 13 Ma (Roger et al., 1995; Wang et al., 2009; Li et al., 2015), with a total offset ~78–100 km (Wang et al., 1998). The dextral strike-slip Sagaing fault (Fig. 1A) was initiated at ca. 11 Ma, with 500 km of displacement resulting from the opening of the Andaman Sea (Curray, 2005; van Hinsbergen et al., 2011b).

The Jinggu Basin is located in the northern part of the Indochina block (Fig. 1A). Sedimentation in the Jinggu Basin is controlled by the Yingpan fault, which is a left-lateral strike-slip fault that runs parallel to the NW-SE Ailao Shan–Red River fault (Fig. 1A). However, when this Yingpan fault was active remains unknown. In the Jinggu area, the fault is separated into series of strands that cut across the Cretaceous–Paleogene redbeds (Fig. 1B). The fault dips to the west in the eastern part of the basin, and to the east in the western part of the basin (Fig. 1B), suggesting that the Jinggu Basin is a pull-apart basin (Tan, 1999).

The Jinggu Basin represents a relatively continuous continental sedimentary succession spanning the Jurassic to Quaternary, preserved in a N-S–trending syncline (YBGMR, 1990; Fig. 1B). The Cenozoic sediments, from old to young, are the Paleocene Mengyejing Formation, the Eocene Denghei Formation, the Eocene to Oligocene Mengla Group, and the middle Miocene Sanhaogou Formation (the ages are based on biostratigraphy that will be described in more detail later herein, when the formations are described). The Mengyejing Formation unconformably overlies Upper Cretaceous sediments and is conformably overlain by the Denghei Formation (Fig. 2). The Mengla Group unconformably overlies the upper Denghei Formation and unconformably underlies the middle Miocene Sanhaogou Formation (Fig. 2). After deposition of the Paleocene Mengyejing Formation and Eocene Denghei Formation, the southeast margin of Tibet experienced significant folding and uplift, mainly in the Eocene, associated with the penetration of India into Asia (He et al., 1996; Schoenbohm et al., 2005; Zhou et al., 2007; Tong et al., 2013; Figs. 1 and 2). This tectonic movement resulted in the widespread deposition of Eocene–Oligocene conglomerates in the eastern Tibetan Plateau, such as the Mengla Group in Jinggu Basin, the Laojunshan Formation in Lanping-Jianchuan Basin, and the Ranmu Formation in the Gongjue Basin and Nangqian Basin (YBGMR, 1990; He et al., 1996; Zhou et al., 2007; for detailed location, see Fig. 1A). In the late Oligocene, after deposition of the Mengla Group, the Jinggu Basin experienced folding again (YBGMR, 1990; Tong et al., 2013; Fig. 2A). Folding of the middle Miocene Sanhaogou Formation occurred in the late Miocene to early Pliocene (He et al., 1996; Fig. 2B).

Sampling

We focused our study on Cenozoic sediments, since there are already many paleomagnetic studies on Cretaceous rocks (e.g., Huang and Opdyke, 1993; Chen et al., 1995; Gao et al., 2015, Fig. 1A).

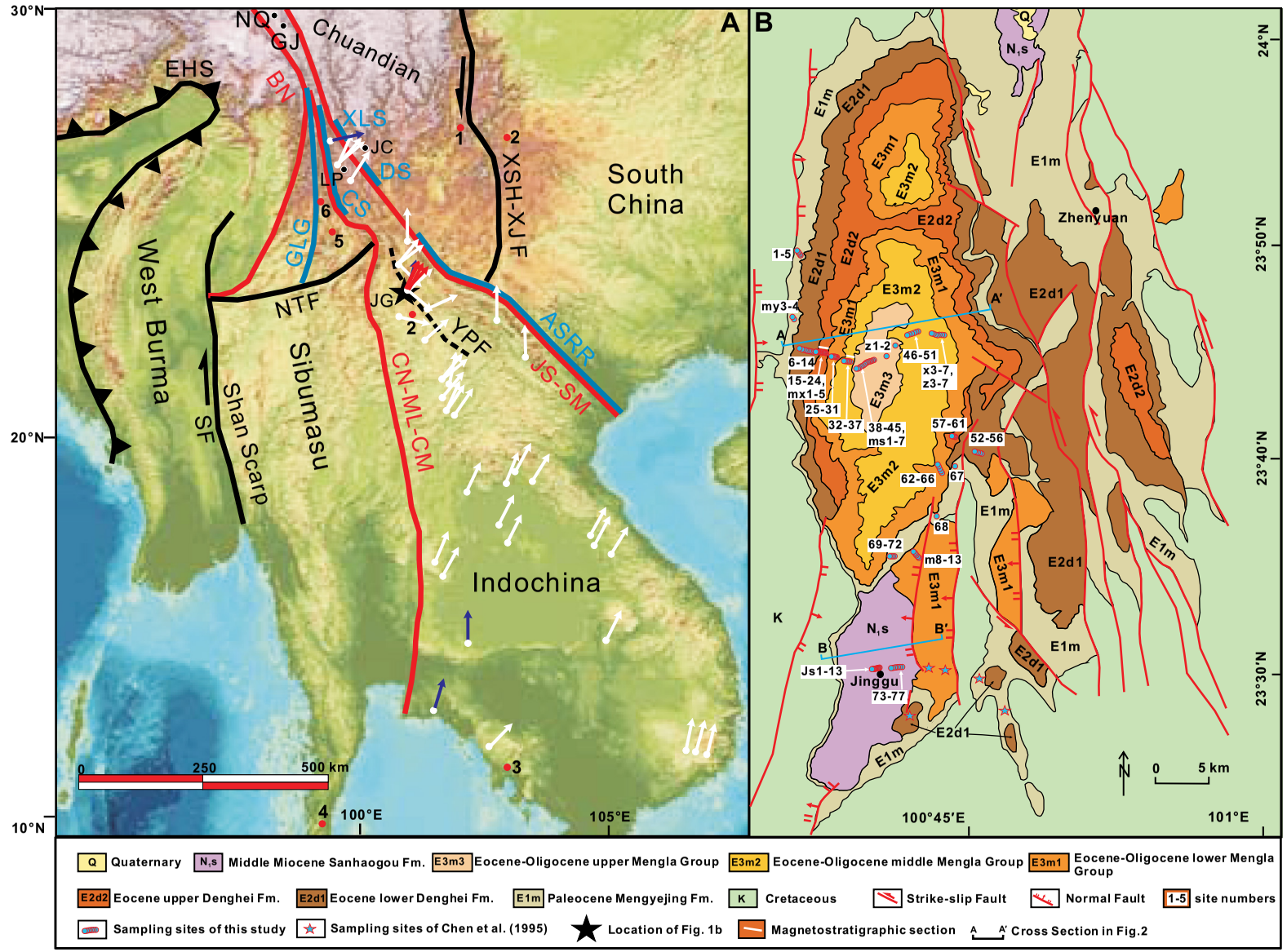

Figure 1. (A) Outline tectonic map of Southeast Asia showing the tectonic framework and major tectonic divisions and (B) simplified geological map of the Jinggu Basin. The white and blue arrows represent the rotation calculated from previous Mesozoic and Cenozoic paleomagnetic results, respectively. The red arrows represent the results of this study. The black star represents the location of Figure 1B. The black dots represent other Cenozoic basins mentioned in the text, while the red dots with numbers represent the remagnetization reported by previous studies. 1—Liu et al. (2011), 2—Huang and Opdyke (2015), 3—Tsuchiyama et al. (2016), 4—Yamashita et al. (2011), 5—Tong et al. (2016), 6—Kornfeld et al. (2014a). Abbreviations: ASRR—Ailao Shan–Red River fault; BN—Bangonghu-Nujiang suture zone; CN-ML-CM—Changning-Menglian-Chiangmai suture zone; CS—Chongshan shear zone; DS—Diancangshan shear zone; EHS—Eastern Himalaya syntaxis; GLG—Gaoligong shear zone; JS-SM—Jinshajiang–Song Ma suture zone; NTF—Nantinghe fault; SF—Sagaing fault; XLS—Xuelongshan shear zone; XSH-XJF—Xianshuihe-Xiaojiang fault; YPF—Yingpan fault; GJ—Gongjue Basin; JC—Jianchuan Basin; JG—Jinggu Basin; LP—Lanping Basin; NQ—Nangqian Basin.

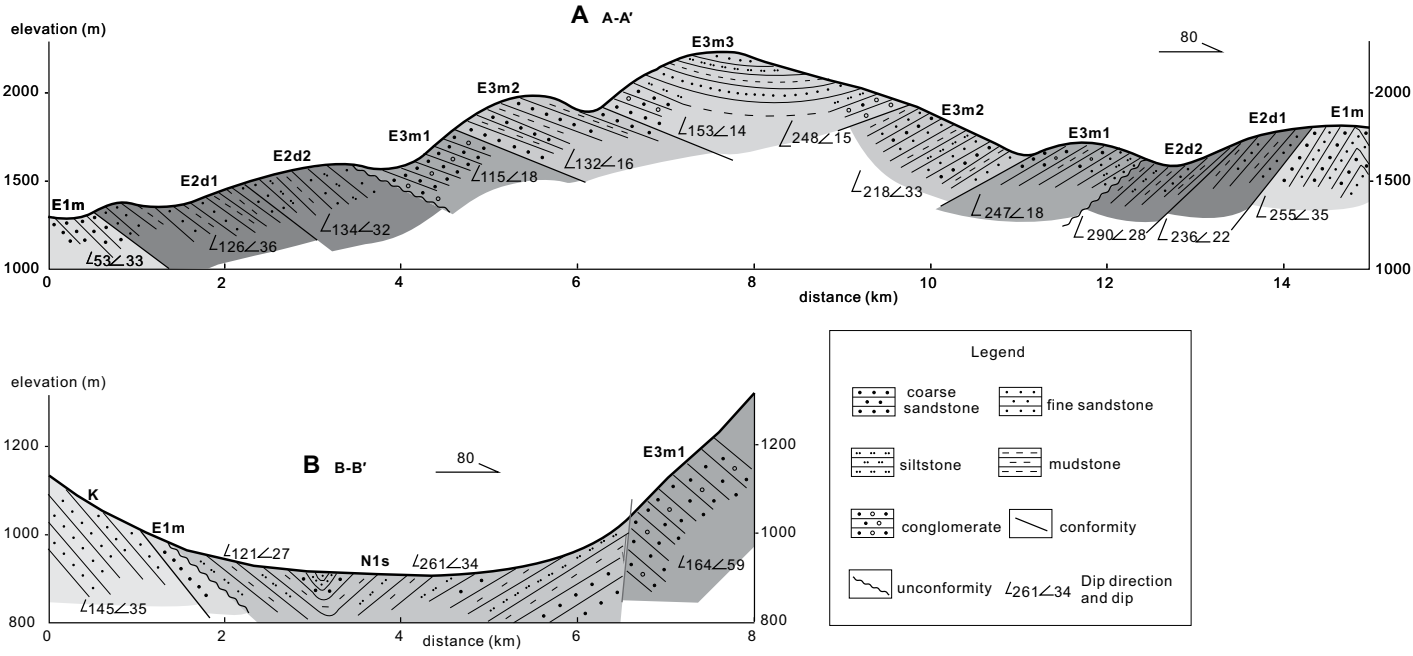

Figure 2. Cross sections from the northern (A-A′) and southern (B-B′) part of the Jinggu Basin. Lettering is the same as Figure 1B.

Our paleomagnetic samples come from the Paleocene Mengyejing Formation (E1m), the Eocene Denghei Formation (E2d), the Eocene to Oligocene Mengla Group (E3m), and the middle Miocene Sanhaogou Formation (N1s; Fig. 1B).

The Mengyejing Formation is dominated by reddish quartz-rich sandstones, mudstones, and muddy gravels. Its age is still to some extent controversial. A Paleocene age was assigned based on its fossil content, such as *Parailyocypris jiangchengensis*, *Qinocypris menglaensis*, *Quadracypris jinghongensis*, and *Cypris yunnanensis* (YBGMR, 1990). However, recent U-Pb ages of 100 Ma to 110 Ma from tuff beds in the Mengyejing Formation in the nearby Jiangcheng Basin suggest a Cretaceous age for the Mengyejing Formation instead (Wang et al., 2015). In total, 13 sites (161 samples) were sampled from this formation, including six sites (72 samples) from the eastern limb of the Jinggu syncline (Fig. 1B).

The Denghei Formation is divided into two units: the lower Denghei Formation (E2d1) and the upper Denghei Formation (E2d2). The lower Denghei Formation is dominated by red fine-grained siltstone beds (0.5–2 m) interbedded with purple red mudstones (0.1–0.5 m); the upper Denghei Formation consists of alternating layers of massive (feldspar- and quartz-dominated) sandstones and mudstones. The age of the Denghei Formation is considered to be Eocene based on stratigraphic considerations, correlations, and its fossil content of ostracods (*Paraleptestheria menglaensis*, *Sinocypris* sp.), charophyta (*Harrisichara yunlongensis*, *Peckichara varians*, and *Stephanochara breviovalis*), gastropods (*Assiminea retopercula*, *Bithynia yunlongensis*), and pollen (YBGMR, 1990). In total, 14 and 20 sites (168 and 238 samples) were sampled on both limbs of the Jinggu syncline from the lower and upper parts of the Denghei Formation, respectively.

The Mengla Group is divided into three parts: the lower (E3m1), middle (E3m2), and upper members (E3m3). The lower Mengla Group is dominated by matrix-supported conglomerates, and massive coarse-grained sandstones interbedded with thin mudstones. The middle Mengla Group mainly contains massive sandstones interbedded with thin mudstones. The lower part of the upper Mengla Group is dominated by gray purple conglomerates, while the upper part is mainly composed of massive gray to reddish sandstones. The Mengla Group is correlated to other conglomerates from the Lanping-Jianchuan Basin, Gongjue Basin, and Nangqian Basin (Zhou et al., 2007; for locations, see Fig. 1A). The $^{40}Ar/^{39}Ar$ dates of volcanic rocks from the Nangqian and Jianchuan Basin at 38–29 Ma (Spurlin et al., 2005; Yang et al., 2014) suggest that the age of the Mengla Group is late Eocene to early Oligocene. In total, 18, 19, and 17 sites (231, 264, and 199 samples) were sampled on both limbs of the Jinggu syncline from the lower, middle, and upper parts of the Mengla Group, respectively.

The Sanhaogou Formation mainly outcrops around Jinggu County (Fig. 1B). It unconformably overlies the Oligocene Mengla Group and is unconformably overlain by unconsolidated Quaternary sands and conglomerates. The Sanhaogou Formation consists of red-grayish to black mudstones, gray and yellow sandstones, several (sandy) conglomerates, and lignites. Besides some ostracods, gastropods, and fish fossils, abundant plant fossils have been found in the Sanhaogou Formation, which is known as the Jinggu flora (YBGMR, 1990). Comparison of the flora assemblages with neighboring areas yields a Miocene age for the Jinggu flora (Wang, 1996; YBGMR, 1990), just slightly older than the Xiaolongtan flora, which was paleomagnetically dated to 13–10 Ma (Li et al., 2015). The age of the Sanhaogou Formation is thus estimated to be middle Miocene. In total, 17 sites (246 samples) were sampled from both limbs of the syncline of the Sanhaogou Formation.

All samples were collected using a gasoline-powered drill and oriented in the field with a magnetic compass. A sun-compass was also used whenever possible. Comparison of orientation data from both methods identified an insignificant declination anomaly, which is in agreement with the value estimated from the geomagnetic map of China 2000 (Xu et al., 2003). In total, 1507 paleomagnetic samples were collected from 118 sites. Each site con-

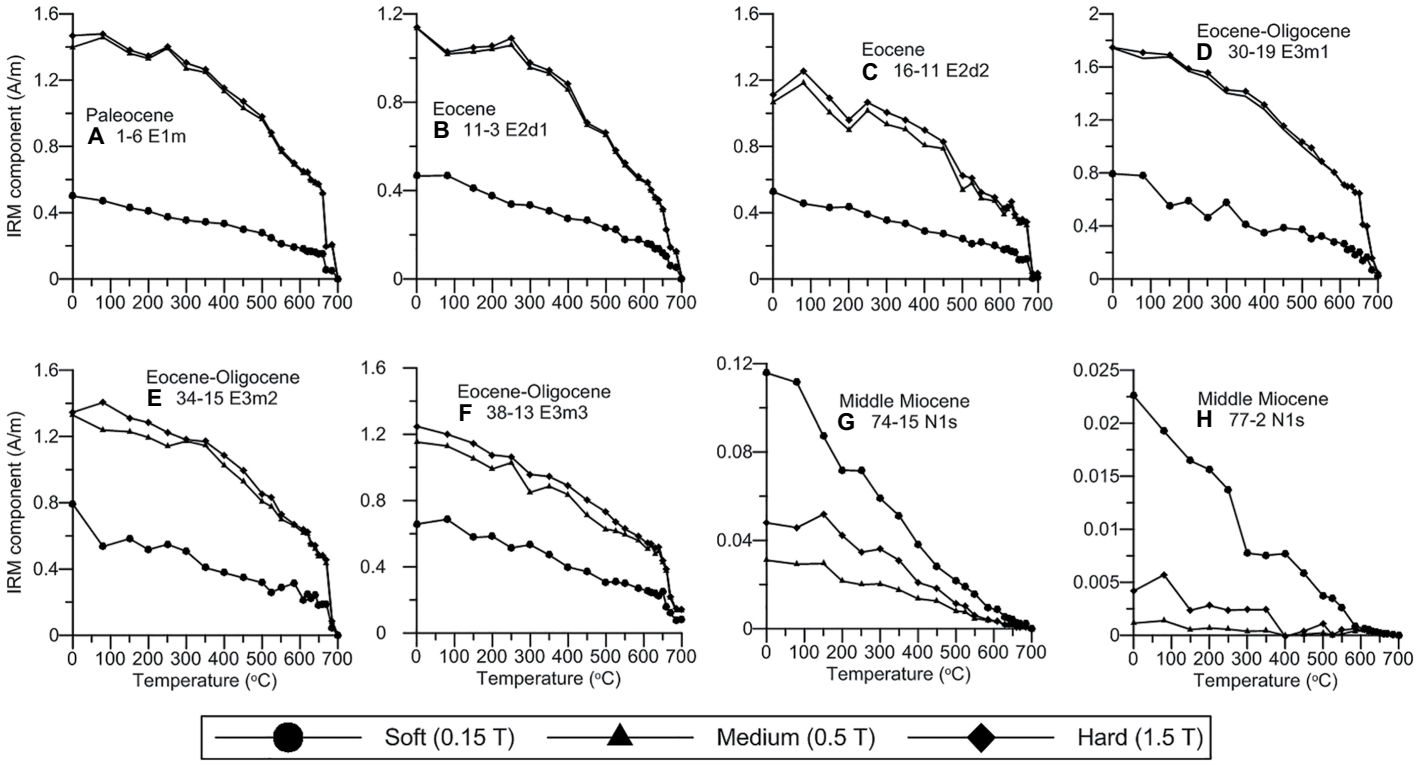

Figure 3. Thermal demagnetization of the composite isothermal remanent magnetization (IRM; imparted with direct current fields of 1.5 T, 0.5 T, and 0.15 T along three perpendicular axes) from (A–F) the Paleogene redbeds and (G–H) the Miocene sandy silts.

tained at least 10 independent samples and spanned a stratigraphic interval of ~2–5 m. In addition, we collected 643 samples from two sections with a sampling interval of ~1 m for magnetostratigraphic purposes (Fig. 1B). All drilled cores were cut into 1–2 specimens (2.5 cm in diameter and 2.2 cm in height) in the laboratory.

PALEOMAGNETISM

Rock Magnetism

To determine the magnetic minerals in the Paleocene–Oligocene redbeds and middle Miocene sandy silts, we measured three-axis isothermal remanent magnetization (IRM; Lowrie, 1990), hysteresis loops, IRM acquisition curves, and direct current (DC) field demagnetization of the saturation IRM (SIRM) on 42 representative samples (eight examples are shown in Figs. 3 and 4). The composite IRMs were acquired with a 2G Enterprises Pulse Magnetizer (2G660). The hard, medium, and soft components were applied in DC fields of respectively 1.5 T, 0.5 T, and 0.15 T along three mutually orthogonal axes. The specimens were then subjected to progressive thermal demagnetization up to 685 °C at 10–50 °C intervals using a thermal demagnetizer (ASC TD-48). Hysteresis loops were measured with a Princeton MicroMag 3900 vibrating sample magnetometer (VSM). The magnetic field was cycled between ±1.5 T. Saturation magnetization (Ms), saturation remanence (Mrs), and coercivity (Bc) were determined after correction for paramagnetic contributions identified from the slope above the field of 1.0 T. Specimens were then demagnetized in alternating fields (AFs) of up to 1.5 T, and an IRM acquisition curve was imparted from 0 to 1.5 T also using the MicroMag 3900 VSM. The SIRM was then demagnetized in a stepwise backfield up to –1.0 T to obtain the coercivity of remanence (Bcr). All the paleomagnetic and mineral magnetic measurements were made in the Paleomagnetism and Geochronology Laboratory (PGL), Beijing, China.

For the Paleogene redbeds, thermal demagnetization curves of the three-component IRM show that all the three components unblock at temperatures of 680–700 °C (Figs. 3A–3F). The intermediate and hard components have a very similar unblocking temperature spectrum, gradually unblocking up to 650 °C, with a higher decay upwards. The soft component more gradually unblocks throughout the entire temperature interval, up to 700 °C. The hysteresis loops are typical of hematite-dominated samples; they are not saturated in fields of 1.5 T (Figs. 4A1–4F1). Also, the IRM acquisition curves show that the magnetic remanence is still not saturated at the maximum applied field of 1.5 T (Figs. 4A2–4F2). The Bcr values (defined with respect to 1.5 T) are as large as 500 mT (e.g., Fig. 4E2), whereas S-ratios (defined as $-IRM_{300\,mT}/IRM_{1\,T}$) are less than 0.4. All of these results are characteristic of a magnetization dominated by high-coercivity hematite. This is confirmed by the IRM component analysis (Kruiver et al., 2001), which suggests that hematite is the dominant magnetic mineral in the redbeds (Figs. 4A3–4F3). It contributes more than 90% to the total IRM (Table DR1[1]).

For the Miocene sandy silts, the three-component IRM is dominated by a soft component, which unblocks fully at temperatures of ~580 °C (Figs. 3G and 3H), indicating the dominance of magnetite. The hysteresis loops and IRM acquisition curves also suggest dominant soft magnetic minerals, as the loops are closed below fields of 0.5 T, and the IRM acquisition curves increase quickly in low fields (Figs. 4G–4H). However, we notice that in some specimens, hematite is also present, because the IRM is still not saturated at the maximum applied field of

[1]GSA Data Repository item 2017144, the original paleomagnetic data and isothermal remanent magnetization (IRM) component analysis results, is available at http://www.geosociety.org/datarepository/2017 or by request to editing@geosociety.org.

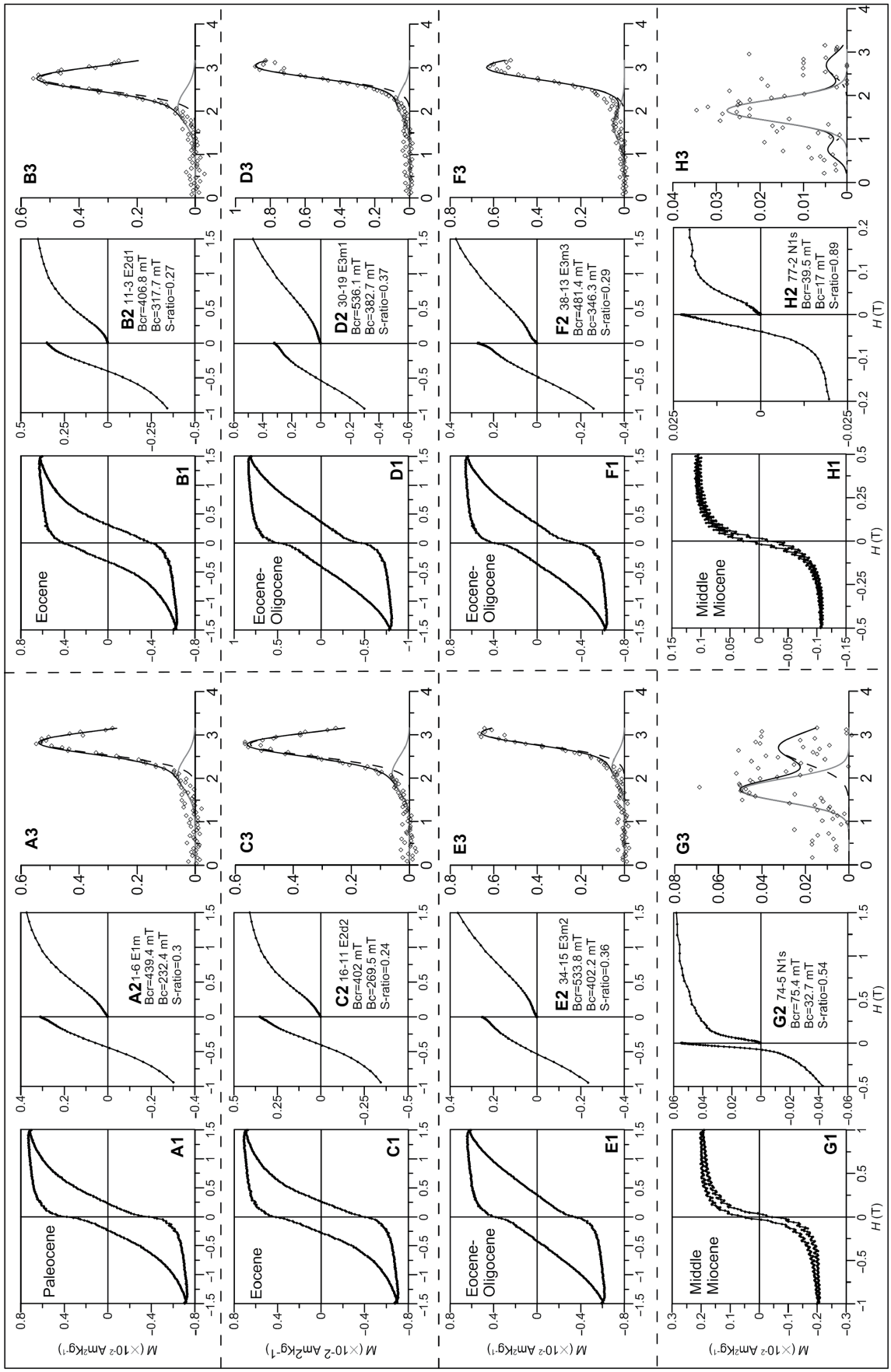

Figure 4. Hysteresis loops (A1–H1), isothermal remanent magnetization (IRM) acquisition and back-field demagnetization curves (A2–H2), and IRM component analysis (A3–H3) from (A–F) the Paleogene redbeds and (G–H) the Miocene sandy silts, where the grey, dashed, and black lines indicate the low-coercivity component, high-coercivity component, and the sum of these components. The open points represent the raw IRM gradient data. Bc—coercivity; Bcr—coercivity of remanence; M—magnetization; H—field; T—tesla; S-ratio— $-IRM_{300\ mT}/IRM_{1\ T}$.

1.5 T (Fig. 4H2). The IRM component analysis also indicates a dominance (~70%; Table DR1 [see footnote 1]) of low-coercivity magnetite and a subdued high-coercivity hematite component (Figs. 4G3–4H3). Therefore, the magnetization of the Sanhaogou Formation is carried by both magnetite and hematite.

Petrography

To investigate the microtexture of the iron oxides, polished thin sections of 36 samples from the Paleogene redbeds were studied using optical and scanning electron microscopy (examples from six representative thin sections are shown in Fig. 5). To further constrain the composition, textural relationships, and origin of the ferromagnetic minerals, we conducted backscattered electron microscopy (BSEM) using a scanning electron microscope (FEI Nova NanoSEM 450) with an energy dispersive spectrometer (EDS; Oxford X-MAX80). Figure 5 depicts examples from the Paleocene Mengyejing Formation (Figs. 5A–5C), for which a Late Cretaceous age is sometimes advocated, the Eocene Denghei Formation (Figs. 5D–5G), and the Mengla Group of Eocene to Oligocene age (Figs. 5H–5O). Most hematite crystals (more than 90%) are subhedral to euhedral; they are distributed either along cracks and pores or around edges of quartz and feldspar grains. They often occur as acicular submicrometer- to micrometer-sized overgrowths on clay minerals (Figs. 5A and 5D), around quartz (Fig. 5B) and feldspars (Fig. 5G), as other silicates (Figs. 5E, 5J, and 5M), as acicular aggregates in pores and voids (Figs. 5D and 5H), replacing and rimming former sulfides (?; Figs. 5I and 5K), and possibly as oxidized framboids (Figs. 5C and 5O). A few (less than 5%) hematite particles could have a detrital origin (Figs. 5F and 5L). Occasionally, manganese oxides were also found to occur as rims and in previously mentioned voids (Fig. 5N).

Demagnetization

The natural remanent magnetization (NRM) of all samples was measured on a 2G Enterprises Model 755 cryogenic magnetometer inside a magnetically shielded room (<300 nT). All specimens from the Paleogene redbeds were subjected to progressive stepwise thermal demagnetization (TD) up to a maximum temperature of 690 °C, with 25–50 °C intervals below 585 °C and 10–15 °C intervals above 585 °C, using an ASC TD-48 thermal demagnetizer with a residual magnetic field less than 10 nT. Both TD and AF demagnetization methods were employed to analyze the specimens from the Miocene sediments.

Demagnetization results were evaluated by orthogonal vector diagrams (Zijderveld, 1967), and the principal component directions were computed by least-squares fits (Kirschvink, 1980). Data analysis was completed using the PaleoMag software (Jones, 2002) and Pmagpy (Tauxe, 2010). Samples with a maximum angular deviation (MAD) larger than 15° were rejected from further analysis. The mean directions were first computed using classic Fisher statistics (Fisher, 1953; Table 1); site mean directions with α_{95} larger than 15° or those falling more than 30° away from the overall mean direction were rejected from further analysis. All the original data are available in the Supplementary Information (see footnote 1) and can be viewed and analyzed online at www.paleomagnetism.org (Koymans et al., 2016).

It has, however, long been recognized (Creer, 1962; Tauxe and Kent, 2004; Tauxe et al., 2008; Deenen et al., 2011) that the distributions of paleomagnetic directions are elongated in the N-S direction. This elongation is dependent on latitude and increases toward lower latitude. This makes the commonly used standard Fisher statistical parameters (α_{95}, k) on direction data sets less appropriate (Tauxe and Kent, 2004). Alternatively, a more robust fit is obtained under the premise of virtual geomagnetic poles (VGPs) being Fisherian-distributed (Tauxe and Kent, 2004; Deenen et al., 2011). Therefore, we also applied Fisher statistics on VGP distributions following the more recent approach of Deenen et al. (2011). In this method, the formation mean directions are calculated for all specimens within a cutoff of 45° around the mean direction. The statistical parameters include ΔD_x, ΔI_x, A95, K, $A95_{max}$, and $A95_{min}$ (Table 2), where ΔD_x and ΔI_x represent the error of declination and inclination, respectively, which are calculated following the method of Butler (1992) as $\Delta D_x = \sin^{-1}(\sin A95/\cos \lambda)$, $\Delta I_x = 2A95/(1 + 3 \sin^2 \lambda)$. A95 and K represent the radius of the 95% confidence limit cone and the precision parameter for the VGP distribution, respectively. $A95_{max}$ and $A95_{min}$ represent the upper and lower limits of an N-dependent A95 reliability envelope to check whether a sample distribution can be straightforwardly explained by paleosecular variation (Deenen et al., 2011).

Paleomagnetic Results

Paleogene Redbeds (Mengyejing Formation, Denghei Formation, Mengla Group)

The NRM intensities of the Paleogene redbeds vary from 2.45×10^{-4} to 2.79×10^{-2} A/m. The demagnetization behavior can be grouped into two types. The first type, including 465 specimens, has only a single univectorial component decaying steadily toward a high temperature of 690 °C (Figs. 6D, 6F, and 6H). The second type, including 621 specimens, shows two components (Figs. 6A–6C, 6I, and 6N). A low-temperature magnetic component was mostly removed below temperature of 300 °C. Above 300 °C, a high-temperature magnetic component decays linearly toward the origin and is regarded as the ChRM. In geographic coordinates, the mean direction of the low-temperature magnetic component coincides with the local geocentric axial dipole field direction (D = 0°, I = 41.4°) at 23.8°N, 100.7°E (Figs. 7A–7F), indicating that the low-temperature magnetic component is probably a recent viscous overprint. For samples from E1m and E3m1, this is not the case.

All ChRMs were isolated between temperatures of 610 °C and 690 °C. Except for a few samples that did not provide interpretable results, most samples (~87%) yielded reliable directions (Table 1). A few sites (e.g., sites 26, 52, 58, and 68) were removed because of their large α_{95} (Table 1). Some of the other sites (e.g., sites 8, 18, and m10–m13) were also discarded because of directions that largely deviated from other sites (Fig. 8; Table 1), which may be due to activity of a local fault close to these site locations (Fig. 1B). The remaining sites were used to calculate the site mean directions (for detailed information, see Table 1).

We note, however, that all directions from Paleogene redbeds were exclusively of normal polarity. Since our paleomagnetic samples were collected at discrete sites, we may coincidentally have missed all the reversed polarity zones. To entirely exclude this (remote) possibility, we performed two high-resolution magnetostratigraphic studies with a sampling interval of ~1 m. One was in the upper part of the Denghei Formation with a thickness of ~500 m, and the other was in the middle part of the Mengla Group with a thickness of ~400 m (for locations, see Fig. 1B). We chose these two parts because the sediments in these two intervals are mostly composed of mudstone and fine sandstone, which generally have relatively low sedimentation rates and consequently have a greater chance to also document reversed polarity zones. All the samples were subjected to the same demagnetization as described before. The conclusion is clear: Both magnetostratigraphic sections yielded only normal polarity directions (Fig. 9).

Neogene Sediments (Sanhaogou Formation)

The NRM intensities of the Sanhaogou Formation range from 1.25×10^{-4} to 9.82×10^{-3} A/m. Stepwise demagnetization isolates either one or two components (Figs. 6O–6R).

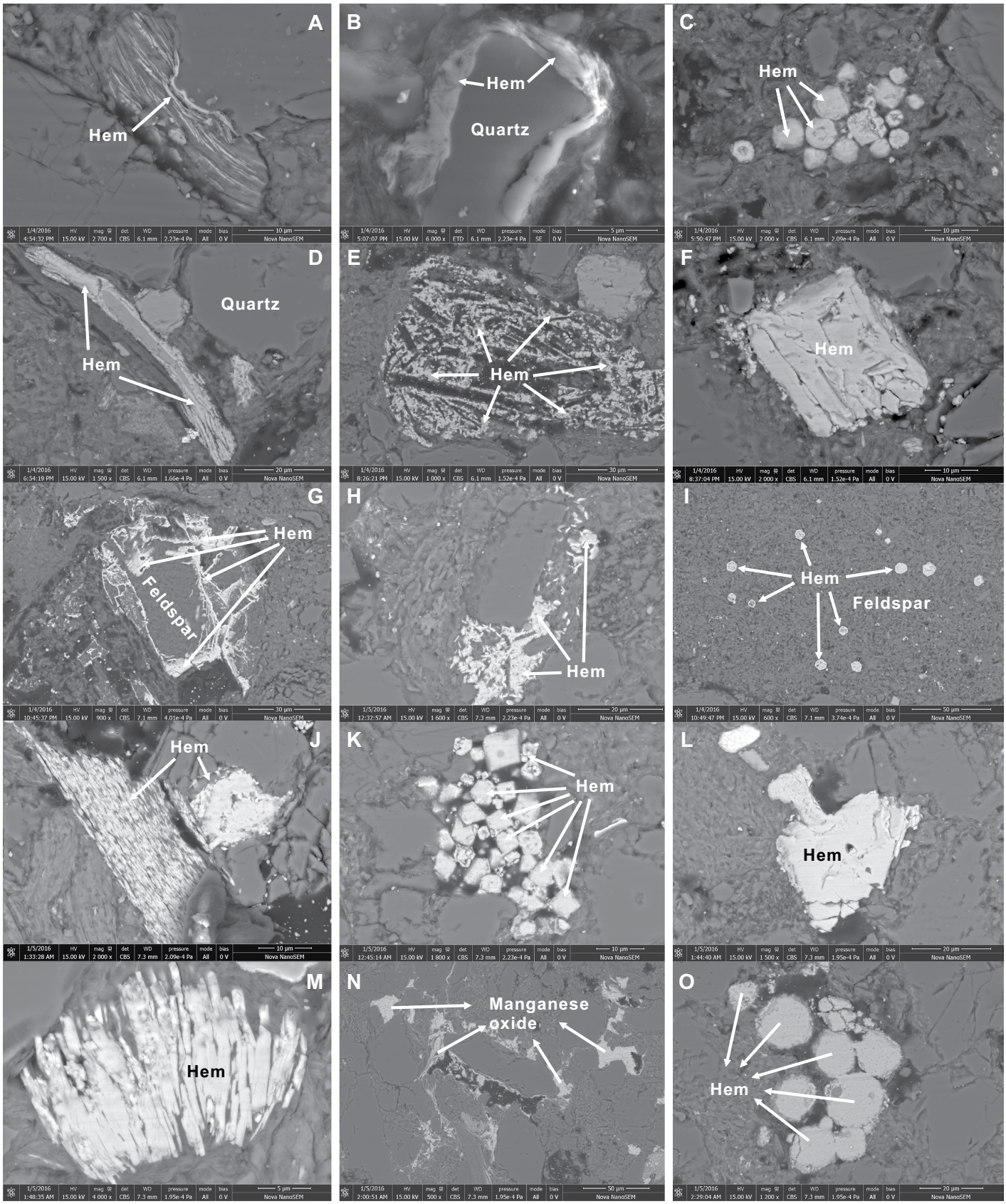

Figure 5. Scanning electron microscope (SEM) backscattered electron images for selected samples of the Paleogene redbeds. Hem—hematite. (A–C) Paleocene Mengyejing Formation, (D–G) Eocene Denghei Formation, (H–O) Eocene–Oligocene Mengla Group.

TABLE 1. SITE-MEAN DIRECTIONS FROM THE CENOZOIC SEDIMENTS FROM JINGGU BASIN (23.7°N, 100.8°E), YUNNAN PROVINCE

		Locality		Bedding		In situ		Tilt-corrected				Tilt-corrected		
Site	Age	Lat (°N)	Long (°E)	dip/dip (°)	*n*0/*n*	D_g (°)	I_g (°)	D_s (°)	I_s (°)	*k*	α_{95} (°)	Plat (°)	Plong (°)	A_{95}
Paleocene Mengyejing Formation (E1m)														
1	E1m	23°49.058′	100°38.281′	55/25	11/12	31.2	58.7	40.1	35	17	11.4	52.6	189.6	
2	E1m	23°49.052′	100°38.274′	53/33	11/12	65	50.2	61	17.7	87.8	4.9	30.1	193.9	
3	E1m	23°49.055′	100°38.265′	53/33	11/12	39.6	55.8	44.8	23.3	119.1	4.2	46.0	197.9	
4	E1m	23°49.055′	100°38.265′	60/30	12/12	29.4	55.9	41	28.4	68	5.3	50.5	195.6	
5	E1m	23°49.039′	100°38.259′	60/30	12/12	27.2	53.6	38.9	26.6	50	6.2	52.1	198.4	
67	E1m	23°39.889′	100°47.175′	6/30	10/12	51.9	49.3	14.7	25.5	11.6	14.8	72.7	224.6	
68*	E1m	23°37.604′	100°45.581′	352/36	10/12	76.4	37.5	54	26.5	9.7	~~16.3~~			
69	E1m	23°35.205′	100°42.822′	298/61	12/12	48	20.5	18.3	26.7	22.7	9.3	70.3	216.2	
70	E1m	23°35.205′	100°42.822′	255/35	12/12	34	21.7	15.7	44.8	19.4	10.1	75.5	176.2	
71	E1m	23°35.219′	100°42.786′	317/40	12/12	57.7	28.6	35	28.1	38.3	7.1	55.9	198.9	
72	E1m	23°35.240′	100°42.808′	295/42	12/12	51.9	23.2	28.2	34.8	55.1	5.9	63.4	194.8	
my3	E1m	23°46.296′	100°37.236′	145/13	12/12	25.6	27.9	32.6	33.6	90	4.6	59.2	194.4	
my4	E1m	23°46.050′	100°37.571′	131/15	12/17	47.3	47.1	62.2	43.5	33.6	7.6	33.9	175.1	
Mean					**12/13**	**43**	**41.7**			19.1	9.8			
								36.1	31.5	27.7	8.4	**55.7**	**194.5**	**8.5**
Eocene Lower Denghei Formation (E2d1)														
6	E2d1	23°44.470′	100°37.937′	51/21	12/12	18.9	51	27.7	32.3	30.4	8	63.4	198.8	
7	E2d1	23°44.473′	100°37.981′	33/15	12/12	26.2	44.8	27.4	29.9	94	4.5	63.2	202.2	
8*	E2d1	23°44.439′	100°38.188′	147/17	12/12	58.8	31.6	68.9	29.6	47	6.4			
9	E2d1	23°44.336′	100°38.534′	67/21	11/12	27.3	41.5	35.3	24.3	29.1	8.6	54.8	202.5	
10	E2d1	23°44.320′	100°38.691′	168/26	11/12	30.5	27.8	45.5	44.9	16.5	11.6	48.9	176.9	
11	E2d1	23°44.304′	100°38.732′	106/44	12/12	10.3	46.8	49.9	34.9	40.5	6.9	43.6	186.1	
12	E2d1	23°44.267′	100°38.756′	145/22	9/12	32.7	23.9	43.6	30.4	60	6.7	48.5	192.5	
13	E2d1	23°44.283′	100°38.832′	108/34	12/12	18.9	35.7	40.6	28.4	210.3	3	50.9	195.7	
14	E2d1	23°44.305′	100°39.095′	126/36	12/12	21.8	41.3	39.9	39.7	39.4	7	53.4	184.3	
52*	E2d1	23°40.677′	100°47.630′	242/23	12/12	53.9	23.7	51.2	46.4	6.1	~~19.2~~			
53	E2d1	23°40.746′	100°47.631′	221/21	12/12	27.7	5.4	24.7	20.9	21	9.7	63.2	215.2	
54	E2d1	23°40.757′	100°47.618′	236/22	11/12	39.4	32.4	26	53.3	10.7	14.6	65.1	160.8	
55	E2d1	23°40.735′	100°47.547′	237/38	12/12	38	2.1	32.7	37.7	39.4	7	59.7	189.1	
56	E2d1	23°40.665′	100°47.623′	221/21	12/12	32	28.5	28.9	49.2	16.8	10.9	63.5	170.5	
Mean					**12/14**	**27.8**	**32.1**			23.2	9.2			
								35.2	35.7	45.5	6.5	**57.2**	**189.6**	**5.7**
Eocene Upper Denghei Formation (E2d2)														
15	E2d2	23°44.304′	100°39.127′	135/34	12/12	34.4	39.6	62.5	37.4	70.6	5.2	32.6	180.2	
16	E2d2	23°44.315′	100°39.176′	116/29	12/12	39.6	38.6	57.3	27.2	36.3	7.3	35.4	189.5	
17	E2d2	23°44.316′	100°39.200′	132/31	12/12	28.9	32.2	49.6	33.7	33.6	7.6	43.6	187.3	
18*	E2d2	23°44.345′	100°39.337′	134/32	12/12	66.1	48.7	88.9	30.3	68	5.3			
19	E2d2	23°44.320′	100°39.424′	124/38	12/12	34	38.5	60.1	29.4	118.7	4	33.3	186.9	
20	E2d2	23°44.272′	100°39.439′	121/38	12/12	36.9	40.8	62.6	27.9	154.8	3.5	30.7	187.0	
21	E2d2	23°44.243′	100°39.460′	130/28	11/12	32.6	33.6	51.2	25.2	25.1	9.3	40.6	193.4	
22	E2d2	23°44.194′	100°39.491′	114/31	11/12	19.7	47.4	50.5	41.1	72.5	5.4	44.0	180.1	
23	E2d2	23°44.330′	100°39.501′	136/32	12/12	41.8	34	62.5	30.4	42.9	6.7	31.3	185.3	
24	E2d2	23°44.280′	100°39.575′	133/42	11/12	24.9	50	73.9	44.6	69.9	5.5	23.9	171.2	
57	E2d2	23°41.121′	100°46.177′	284/33	11/12	57.5	14.6	45	35	24.6	9.4	48.1	187.8	
58*	E2d2	23°41.098′	100°46.189′	298/32	11/12	47.8	6.4	41.6	15.9	7.6	~~17.7~~			
59	E2d2	23°41.023′	100°46.147′	290/28	12/12	64.2	11.5	55.9	29.7	32.7	7.7	37.1	188.3	
60	E2d2	23°41.040′	100°46.192′	275/26	11/12	42.9	18.8	32	32.9	60.9	5.9	59.6	195.6	
61	E2d2	23°41.048′	100°46.204′	292/29	10/12	51.1	22.8	36.2	33.8	21.3	10.7	55.9	192.5	
mx1	E2d2	23°44.457′	100°39.505′	128/42	10/10	18.4	38.1	54.3	39.5	43.6	7.4	40.3	180.7	
mx2	E2d2	23°44.457′	100°39.505′	128/42	14/14	32	31.3	56.3	26.5	14	11	36.2	190.3	
mx3	E2d2	23°44.498′	100°39.440′	149/26	11/11	37	25.9	51.4	32.7	14.3	12.5	41.8	187.5	
mx4	E2d2	23°44.504′	100°39.436′	141/34	13/13	29.7	22.2	46.6	30.1	11.6	12.7	45.7	191.6	
mx5	E2d2	23°44.374′	100°39.435′	130/26	9/10	23.9	39.9	47	42.1	42.4	8	47.3	179.9	
Mean					**18/20**	**37**	**32.8**			29	6.5			
								53	33.6	66.6	4.3	**40.5**	**186.0**	**4.3**
Eocene–Oligocene Lower Mengla Group (E3m1)														
25	E3m1	23°44.154′	100°39.995′	85/25	12/12	11.9	25.5	21	16.2	20.2	9.9	64.6	224.8	
26*	E3m1	23°43.956′	100°40.019′	115/18	8/12	20.9	38.8	35.2	37.8	13.7	~~15.5~~			
27	E3m1	23°43.849′	100°40.007′	115/18	12/12	8.1	45.2	27.1	47.6	22.7	9.3	65.2	173.2	
28	E3m1	23°43.650′	100°40.014′	130/23	12/12	44.7	46.9	68.6	39.5	15.5	11.4	27.5	176.8	
29	E3m1	23°43.556′	100°40.077′	155/10	11/12	30.8	29.2	36.1	34.5	26.1	9.1	56.1	191.7	
30	E3m1	23°43.586′	100°40.215′	105/15	12/12	20.5	45.6	34.7	42.3	24.7	8.9	58.4	182.1	
31	E3m1	23°43.634′	100°40.341′	86/16	12/12	24.4	32.6	31.8	24.1	12.5	12.8	57.9	205.3	
62	E3m1	23°39.857′	100°45.516′	282/27	10/12	48.7	48.2	24.1	61.2	50	6.9	62.7	141.9	
63	E3m1	23°39.799′	100°45.545′	238/15	12/12	38.2	20.1	34.8	32.3	29	8.2	56.9	194.8	
64	E3m1	23°39.805′	100°45.568′	234/14	7/12	60.7	11	61.3	24.9	22.8	12.9	31.3	189.5	
65	E3m1	23°39.793′	100°45.603′	250/18	10/12	46.7	24.6	41.5	40.8	54.5	6.6	52.1	182.6	
66	E3m1	23°39.804′	100°45.629′	250/14	10/12	42.1	25.6	37.8	37.7	21	10.8	55.1	187.3	
m8*	E3m1	23°35.958′	100°43.784′	165/41	17/17	35.7	27.5	65	45.8	23	7.6			
m9*	E3m1	23°35.975′	100°43.773′	151/37	6/16	23.7	30.6	51.8	46.1	13.3	~~19.1~~			
m10*	E3m1	23°35.995′	100°43.752′	155/45	14/14	56.3	36.6	88	30.6	22.3	8.6			
m11*	E3m1	23°36.001′	100°43.721′	166/49	14/14	69	46.7	112.1	32.7	137.6	3.4			
m12*	E3m1	23°35.987′	100°43.685′	164/59	13/13	44.8	21.4	79.6	35.2	24.8	8.5			
m13*	E3m1	23°36.010′	100°43.684′	165/55	13/13	46.9	29.1	86.9	38	11.6	12.7			
Mean					**11/18**	**34.9**	**33.2**			19.1	10.7			
								38.4	37.3	22.9	9.7	**54.8**	**186.2**	**9.4**

(*continued*)

TABLE 1. SITE-MEAN DIRECTIONS FROM THE CENOZOIC SEDIMENTS FROM JINGGU BASIN (23.7°N, 100.8°E), YUNNAN PROVINCE (*continued*)

		Locality		Bedding		In situ		Tilt-corrected				Tilt-corrected		
Site	Age	Lat (°N)	Long (°E)	dip/dip (°)	*n*0/*n*	D_g (°)	I_g (°)	D_s (°)	I_s (°)	*k*	α_{95} (°)	Plat (°)	Plong (°)	A_{95}
Eocene–Oligocene Middle Mengla Group (E3m2)														
32	E3m2	23°43.630′	100°40.416′	132/16	11/12	29	27.2	37.6	29.6	17.6	11.2	53.9	196.2	
33	E3m2	23°43.639′	100°40.763′	108/23	12/12	20.5	46.4	42.3	40.9	15.5	11.4	51.4	182.3	
34	E3m2	23°43.624′	100°40.870′	98/23	8/12	21.9	40.7	37.8	31.9	83.4	6.1	54.1	193.8	
35	E3m2	23°43.549′	100°40.843′	105/21	11/12	20.7	29.8	31.7	25.6	35.2	7.8	58.3	203.9	
36	E3m2	23°43.545′	100°40.942′	107/32	12/12	354.9	44.4	29.2	47.4	14	12	63.4	174.0	
37	E3m2	23°43.641′	100°41.519′	125/31	12/12	33.8	47.6	63.7	39.8	24.2	9	31.9	177.9	
46	E3m2	23°46.044′	100°44.042′	248/15	12/12	37.7	14.6	34.6	27.4	57	5.8	56.1	200.2	
47	E3m2	23°46.096′	100°44.156′	271/21	12/12	40.8	18.3	35.5	36.7	40.5	6.9	57.0	189.5	
48	E3m2	23°46.162′	100°44.154′	271/27	10/12	35.3	19.3	28.8	36.6	46	7.2	63.1	192.3	
49	E3m2	23°45.749′	100°45.819′	255/26	10/12	44.4	6.5	39.8	28.5	21.7	10.6	51.6	196.2	
50*	E3m2	23°45.777′	100°46.104′	218/33	10/12	4.9	23.5	348.5	48.9	20.6	10.9			
51*	E3m2	23°45.777′	100°46.104′	218/33	10/12	6.5	–0.6	2.1	27.1	35.7	8.2			
x3	E3m2	23°45.935′	100°46.037′	209/37	10/18	50.6	–15.4	51	19.1	16.4	12.3	39.5	197.8	
x4	E3m2	23°45.951′	100°46.037′	207/32	9/14	35.4	6.3	37.6	37.9	27.5	10	55.3	187.3	
x6	E3m2	23°45.360′	100°46.788′	245/32	6/12	53.1	–21.1	53.6	10.3	296.1	3.9	35.3	201.7	
x7	E3m2	23°45.190′	100°46.026′	257/34	12/16	39.5	–1.7	34.9	24.8	44.2	6.6	55.3	202.5	
z3	E3m2	23°46.252′	100°44.083′	264/17	13/17	48.8	21.1	43.2	34.5	21.3	9.2	49.6	189.0	
z4+6	E3m2	23°46.106′	100°44.594′	265/24	7/30	40.2	21.5	29.7	37	22.2	13.1	62.4	191.4	
z7	E3m2	23°46.064′	100°44.862′	242/24	9/13	30.5	27.1	19.5	46.5	27.5	10	72.0	173.7	
Mean					**17/19**	**35.2**	**20.2**			12.1	10.7			
								38.6	33	40	5.7	**53.9**	**191.8**	**5.1**
Eocene–Oligocene Upper Mengla Group (E3m3)														
38	E3m3	23°43.912′	100°42.262′	153/14	10/12	24.9	18.6	29.6	26.8	181	3.6	60.5	204.1	
39	E3m3	23°44.085′	100°42.375′	211/14	12/12	48.2	12.4	49.7	25.8	31.9	7.8	42.1	193.5	
40	E3m3	23°44.225′	100°42.719′	205/11	9/12	42.7	16.8	44.1	27.2	31.6	9.3	47.5	195.0	
41	E3m3	23°44.605′	100°43.117′	155/16	10/12	45.1	23	52.4	27.5	81	5.4	39.9	191.2	
42	E3m3	23°44.768′	100°43.047′	166/9	11/12	48.1	22.4	51.8	26.3	37.1	7.6	40.3	192.3	
43	E3m3	23°44.950′	100°42.959′	189/13	12/12	43.7	44.1	53.3	54.2	42.9	6.7	42.8	164.4	
44	E3m3	23°45.221′	100°43.052′	154/13	11/12	42.7	43.6	55.4	47	23.6	9.6	40.4	173.0	
45	E3m3	23°45.817′	100°43.990′	229/14	12/12	58.9	17.4	60.1	31.2	44.2	6.6	33.6	185.6	
ms1*	E3m3	23°44.367′	100°42.652′	164/19	0/10									
ms2*	E3m3	23°44.347′	100°42.611′	148/15	8/12	44.6	42.3	58.7	44	12.8	~~16.1~~			
ms3	E3m3	23°44.249′	100°42.308′	184/21	10/12	39.8	18.6	46.6	35	18.3	11.6	46.6	187.2	
ms4	E3m3	23°44.172′	100°42.199′	169/12	9/12	52.5	9.5	54.8	14.6	33	9.1	35.1	198.5	
ms5	E3m3	23°44.071′	100°42.197′	177/16	12/13	42.6	23.4	49.2	34	14	12	44.1	187.2	
ms6	E3m3	23°43.790′	100°41.424′	136/12	7/10	54.4	31.6	61.3	29.2	17.6	14.8	32.1	186.5	
ms7*	E3m3	23°43.706′	100°40.882′	116/32	0/8									
z1	E3m3	23°43.767′	100°43.141′	194/20	11/14	51.8	13.7	56.9	29	29.8	8.5	36.1	188.3	
z2	E3m3	23°44.852′	100°42.961′	158/29	9/12	33.3	21.3	47.4	35.1	19.1	12.1	45.9	186.8	
Mean					**14/17**	**45**	**22.8**			37.5	6.6			
								50.8	31.8	47.7	5.8	**43.1**	**187.9**	**5.2**
Middle Miocene Sanhaogou Formation (N1s)														
73*	N1s	23°30.548′	100°42.549′	236/35	12/12	343.8	41.1	311.3	42.1	61	5.6			
74	N1s	23°30.546′	100°42.550′	256/34	8/12	24	22.6	5.4	39.5	83.4	6.1	84.9	202.0	
75	N1s	23°30.398′	100°41.921′	249/26	12/12	15.8	13.1	7.5	27.4	279.7	2.6	78.6	241.0	
76*	N1s	23°30.381′	100°41.875′	262/57	0/12									
77*	N1s	23°30.338′	100°41.352′	260/29	8/12	265	–28.8	268.2	–57.7	57	7.4			
JS1	N1s	23°30.677′	100°44.146′	206/27	13/13	185.3	–8	181.4	–33	14	11.5	84.3	267.0	
JS2	N1s	23°30.739′	100°43.470′	206/27	8/22	21	–11.9	21	15	24.2	11.5	64.4	225.4	
JS3	N1s	23°30.600′	100°43.224′	121/27	12/13	3.6	29.9	21.5	38.7	736.9	1.6	70.1	191.2	
JS4	N1s	23°30.601′	100°43.231′	114/24	13/13	5.5	26.9	19	31.9	356	2.2	71.2	206.3	
JS5	N1s	23°30.602′	100°43.241′	114/23	12/12	9	27	21.7	30.6	61	5.6	68.5	205.6	
JS6*	N1s	23°30.603′	100°43.250′	229/39	6/10	22.3	11.2	348.3	35.1	7.9	~~25.5~~			
JS7	N1s	23°30.606′	100°43.261′	224/31	10/14	20.6	3.3	16.3	31.4	102.3	4.8	73.4	210.7	
JS8+9	N1s	23°30.842′	100°42.592′	261/34.3	11/30	23.5	17.5	8.5	32.5	27.9	8.8	80.1	225.3	
JS10*	N1s	23°30.681′	100°42.259′	251/48	7/16	8.6	38.3	323.6	43.3	46	9			
JS11*	N1s	23°30.568′	100°41.857′	298/40	14/15	10.4	13	6.3	–0.9	75.6	4.6			
JS12	N1s	23°30.538′	100°41.315′	263/48	7/15	213.9	–14.4	191.1	–39.6	17.6	14.8	88.6	235.8	
JS13*	N1s	23°30.496′	100°42.565′	270/35	0/13									
Mean					**10/17**	**16.4**	**15.4**			25.8	9.7			
								13.5	32.2	71.2	5.8	**77.0**	**214.9**	**5.5**

*Note: n*0/*n*—number of specimens used to calculate the site or formation mean direction/number of demagnetized specimens; Dg/Ds—declination in geographical/stratigraphical coordinates; Ig/Is—inclination in geographical/stratigraphical coordinates; *k*—precision parameter; α_{95}—radius of the 95% confidence cone about site-mean direction; Plat/Plon—virtual geomagnetic pole latitude/longitude; A95—radius of 95% confidence circle around paleomagnetic pole. Numbers that are struck through—site confidence limits larger than 15°.

*Denotes the sites that were excluded from calculating the formation mean directions.

The low-temperature magnetic component was mostly isolated at temperature intervals of 20–250 °C or at fields between 5 and 20 mT, while the ChRM was separated between temperatures of 300–400 °C and 500–550 °C or 610 °C and 680 °C, or between fields of 30 mT and 60 mT. In geographic coordinates, the mean direction of the low-temperature magnetic component has a similar declination but much shallower inclination compared with the local geocentric axial dipole field direction ($D = 0°$, $I = 41.4°$) at 23.8°N, 100.7°E (Fig. 7G). The intensity of specimens from site JS13 increased one order of magnitude after 250 °C demagnetization, and directional behavior became erratic, indicating neoformation of highly magnetic minerals. The intensities of specimens from site JS17 decreased quickly to less than 10% of the NRM

TABLE 2. FORMATION MEAN DIRECTIONS OF THE CENOZOIC SEDIMENTS FROM JINGGU BASIN USING THE METHOD OF DEENEN ET AL. (2011)

Formation name	Age	*n*0/*n*	*N*	*D*	Δ*Dx*	*I*	Δ*Ix*	*K*	A95	$A95_{min}$	$A95_{max}$
Geographic coordinates											
E1m	Paleocene	143/149	161	44.2	3.4	40.9	4.2	15.6	3.1	1.6	3.6
E2d1	Eocene	146/151	168	27.5	3.0	31.2	4.5	18.0	2.8	1.6	3.6
E2d2	Eocene	224/230	238	38.0	2.3	32.8	3.4	19.9	2.2	1.4	2.7
E3m1	Eocene–Oligocene	124/128	144	33.0	3.8	33.9	5.5	13.3	3.6	1.7	3.9
E3m2	Eocene–Oligocene	190/200	264	33.6	2.7	20.1	4.8	16.1	2.6	1.5	3.0
E3m3	Eocene–Oligocene	152/154	199	45.2	2.5	23.6	4.3	22.4	2.5	1.6	3.5
N1s	Middle Miocene	124/153	246	14.6	2.6	17.0	4.9	29.0	2.6	1.9	4.3
Tectonic coordinates											
E1m	Paleocene	146/149	161	38.1	2.8	31.0	4.4	19.4	2.7	1.6	3.6
E2d1	Eocene	142/151	168	37.4	2.7	35.2	3.9	22.0	2.6	1.7	3.6
E2d2	Eocene	224/230	238	54.7	2.1	32.8	3.2	22.2	2.0	1.4	2.7
E3m1	Eocene–Oligocene	120/128	144	34.9	3.3	36.4	4.6	18.0	3.1	1.8	4.0
E3m2	Eocene–Oligocene	191/200	264	36.1	2.6	33.5	3.8	17.8	2.5	1.5	3.0
E3m3	Eocene–Oligocene	152/154	199	51.2	2.7	32.6	4.0	21.1	2.6	1.6	3.5
N1s	Middle Miocene	108/153	246	13.6	2.5	32.4	3.8	33.7	2.4	1.9	4.4

*Note: n*0/*n*—number of specimens used to calculate the formation mean direction/number of specimens that yield interpretable results; *N*—number of demagnetized specimens; *D*—declination; Δ*Dx*—error on declination; *I*—inclination; Δ*Ix*—error in inclination. Statistical parameters are given by a confidence cone using Fisher (1953) statistics on virtual geomagnetic poles (A95, *K*). $A95_{min}$ and $A95_{max}$ correspond to the confidence envelope of Deenen et al. (2011).

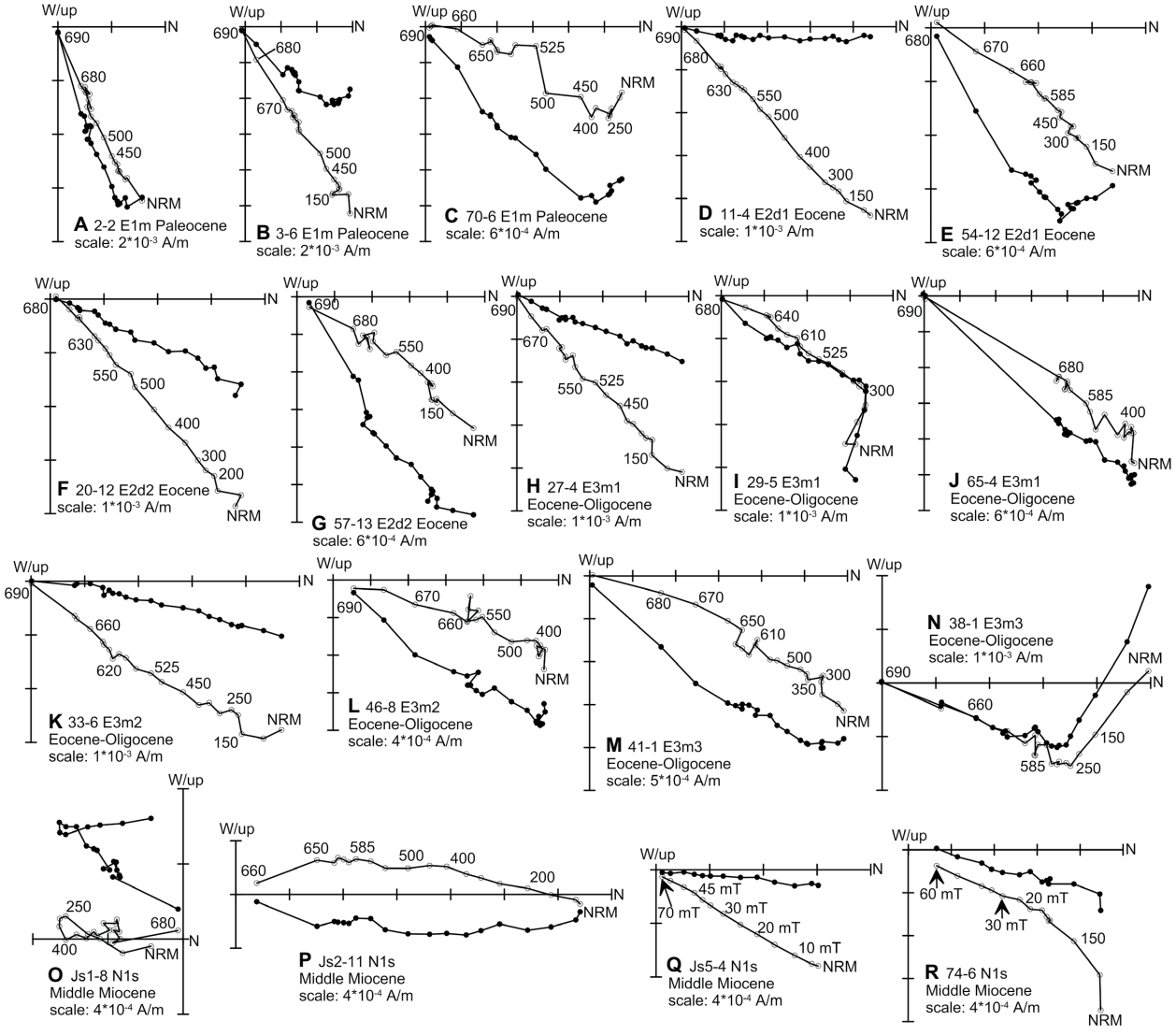

Figure 6. Orthogonal vector projections of demagnetization for (A–N) Paleogene and (O–R) Miocene specimens in geographical coordinates. Solid and open symbols refer to vector projected onto the horizontal and vertical planes, respectively. NRM—natural remanent magnetization.

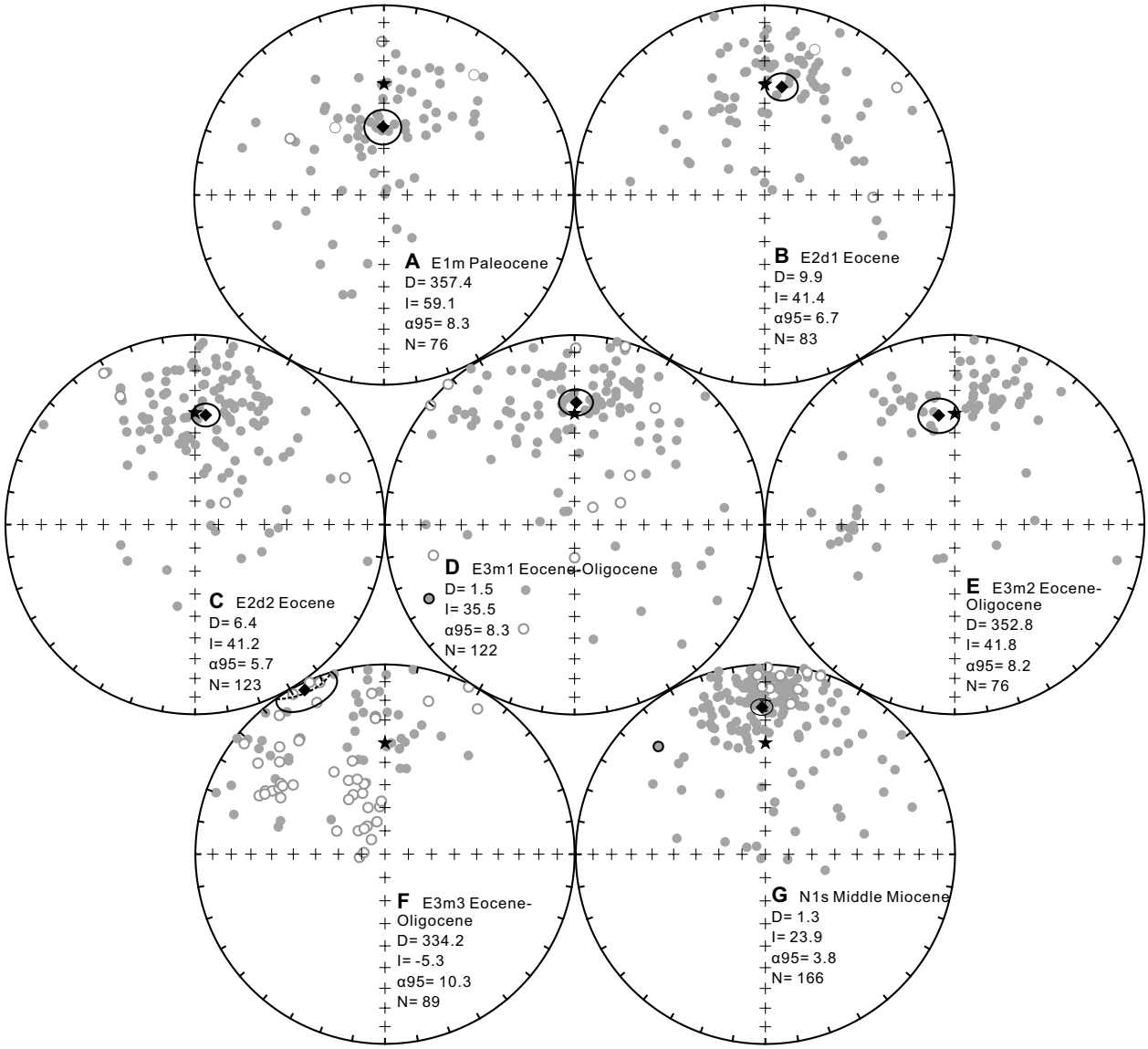

Figure 7. Equal-area projections of the site-mean directions of the low-temperature component (LTC) in situ for (A) Paleocene, (B–C) Eocene, (D–F) Eocene-Oligocene, and (G) Miocene specimens. Solid (open) symbols refer to positive, downward (negative, upward) inclinations; black diamond indicates overall mean direction with 95% confidence limits; and star indicates the geocentric axial dipole field direction at the sampling site. D—declination; I—inclination; α95—radius of the 95% confidence cone about mean direction; N—specimen number.

after 30–40 mT AF demagnetization; above this field, the demagnetization behavior became erratic. No meaningful results could be obtained from these two sites. Sites JS6, JS10, JS11, JS14, and JS18 were excluded either because of large α95 or large deviation from the other site mean directions (Fig. 8G). Sites JS8 and JS9 were combined into one site. The remaining 10 sites had dual polarity (Fig. 8G). After inverting the reversed directions, they have a mean direction of D_g = 16.4°, I_g = 15.4°, kg = 25.8, $\alpha95_g$ = 9.7° before tilt correction and D_s = 13.5°, I_s = 32.2°, k_s = 71.2, $\alpha95_s$ = 5.8° after tilt correction (Fig. 8G), where subscripts g and s indicate the values in geographical and stratigraphical coordinates, respectively. This is consistent with the middle Miocene result of Gao et al. (2015).

DISCUSSION

Reliability of the Paleomagnetic Directions

To assess the primary nature of the ChRM, the fold tests of McElhinny (1964) and McFadden (1990) were conducted. The nonparametric incremental fold test of Tauxe and Watson (1994) was also employed to check the best grouping of the data set as a function of the percentage of unfolding. As shown in Table 3, both the fold tests of McElhinny (1964) and McFadden (1990) applied to the Mengyejing and lower Denghei Formations were indeterminate, although the precision parameters (k) increased after tilt correction. This was confirmed by the nonparametric incremental fold test, which shows the synfolding character as well, with the best grouping of the formation mean directions occurring at 52%–78% unfolding (Figs. 10A and 10B). The mean directions of the other Paleogene formations, however, passed the fold test of McElhinny (1964), that of McFadden (1990), or both (Table 3). The best grouping of the formation mean directions occurs at 72%–113%

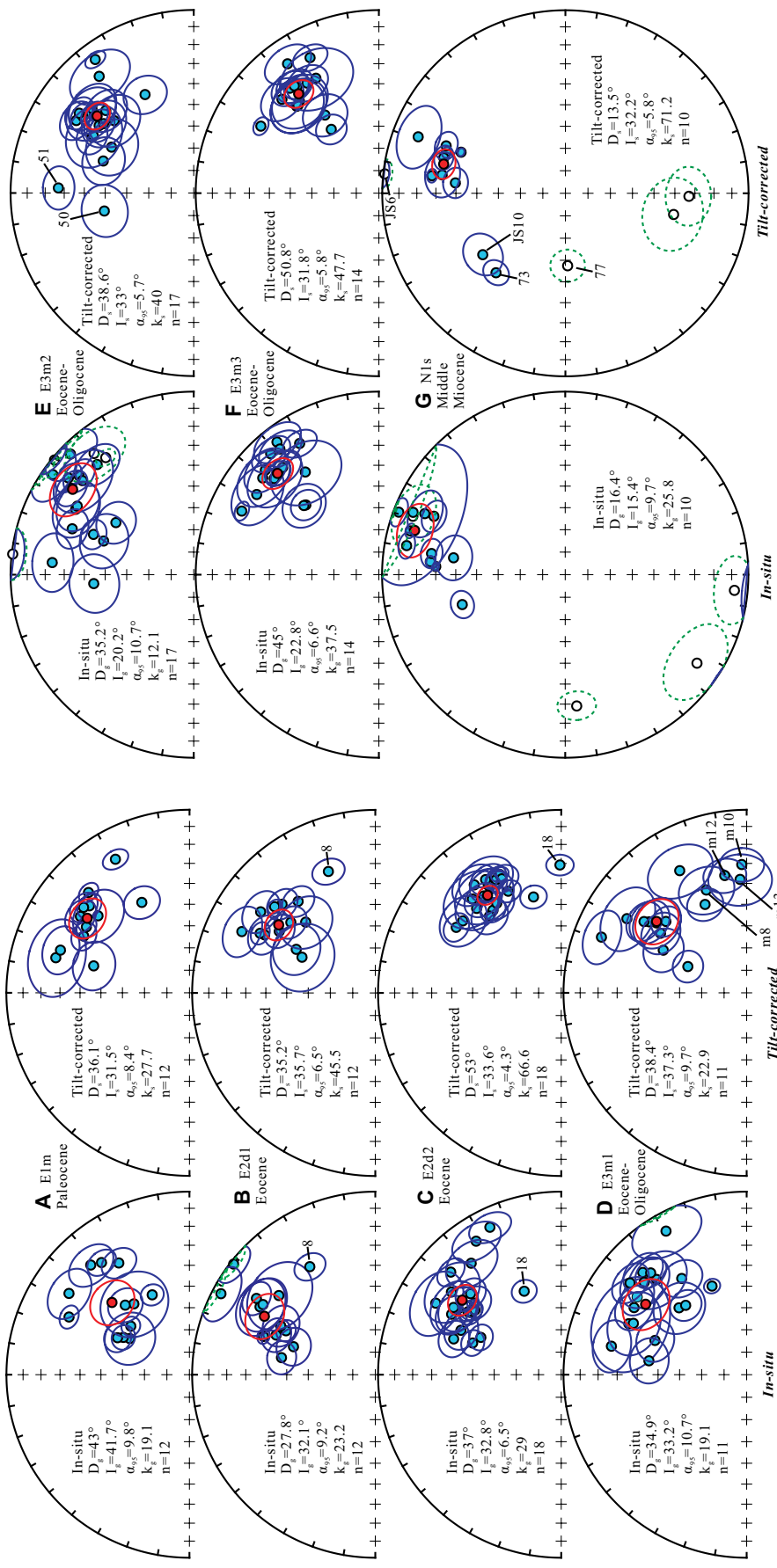

Figure 8. Equal-area projections of formation mean directions of the high-temperature characteristic remanent magnetization (ChRM) for in situ and tilt-corrected coordinates. Solid (open) symbols refer to positive, downward (negative, upward) inclinations; red dots indicate overall mean directions with 95% confidence limits. Sites with numbers were excluded from calculating the mean directions (Table 1). D—declination; I—inclination; α95—radius of the 95% confidence cone of site mean directions; n—site number; kg/ks—precise parameter in in-situ and tilt-corrected coordinates, respectively.

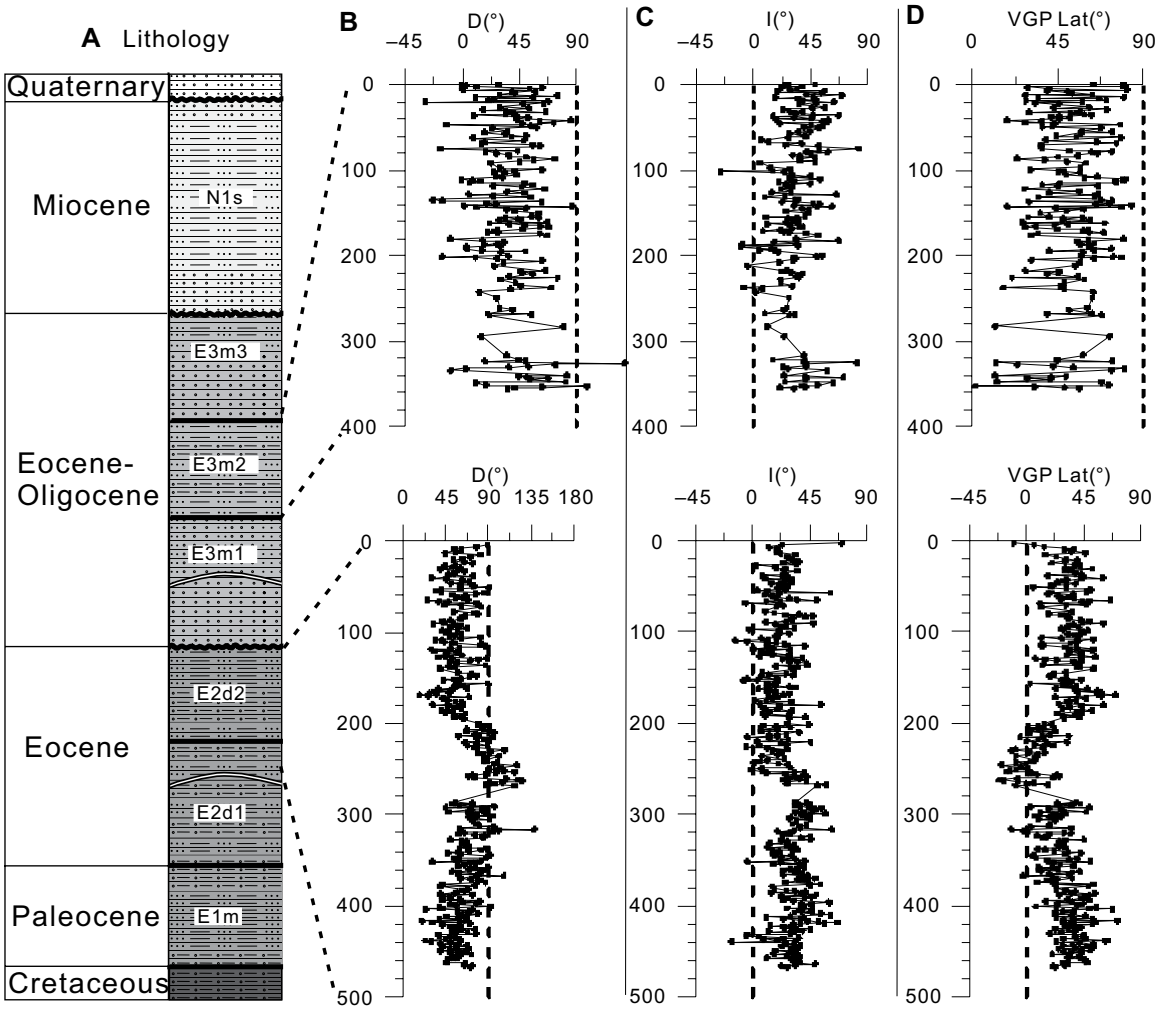

Figure 9. (A) Lithology and (B–D) magnetostratigraphic results of the two studied sections. D—declination; I—inclination; VGP Lat—virtual geomagnetic pole latitude. All polarities appear to be normal. The curved white lines in E3m1 and E2d1 represent deposition hiatuses. The lithology and lettering in column A are the same as Figure 2.

unfolding (Figs. 10C–10F), which is essentially indistinguishable from the mean directions after 100% unfolding, suggesting a prefolding origin of the ChRMs. Whether this would imply a primary NRM is discussed in the next section.

The fold test of the Neogene Sanhaogou Formation was positive at the 95% probability level (Table 3), according to the fold tests of McElhinny (1964) and McFadden (1990). The fold test of Tauxe and Watson (1994) showed that the best grouping of the mean ChRM directions occurs at ~74%–92% unfolding (Fig. 10G), which is statistically identical to the mean direction after 100% unfolding. The antipodal directions also pass the reversals test of McFadden and McElhinny (1990) at the 95% probability level and the bootstrap reversals test (Tauxe, 2010; Fig. 10H). Thus, the ChRM of the Sanhaogou Formation most likely represents a primary NRM.

Primary Magnetization or Magnetic Overprint of the Paleogene Redbeds?

The positive fold tests from the Paleogene redbeds indicate a prefolding magnetization, frequently interpreted to suggest its primary nature. However, we note that all the magnetic directions isolated from the redbeds, including those from the two sections sampled in high resolution, are exclusively of normal polarity, whereas reversed polarity occupies more than half of the early Cenozoic Epoch (e.g., Ogg, 2012). Therefore, the ChRMs obtained from the redbeds are prefolding, but they most likely do not represent a primary NRM.

In this debate, the age assignment of the successions is central. The Paleogene age determination for the sedimentary successions of the Jinggu Basin, however, is not beyond discussion, and in particular, the age of the lowermost Mengyejing Formation is debated (YBGMR, 1990; Chen et al., 1995; Wang et al., 2015). Recently, some intercalated volcanic tuff beds from this formation provided U-Pb ages of 110–100 Ma in the Jiangcheng Basin, ~200 km southeast of our studied area (Wang et al., 2015). These U-Pb ages suggest that the Mengyejing Formation would be Cretaceous in age instead of Paleocene. If the dating of tuff beds at 110–100 Ma by Wang et al. (2015) from the Mengyejing Formation is representative of a Cretaceous age for the entire redbed sequence, the prefolding ChRMs could be primary magnetizations acquired during sediment deposition in the Cretaceous normal superchron (121–83 Ma). A primary NRM would explain the inclination bias with respect to Eurasia (Table 3), because inclination shallowing is frequently observed in redbeds (e.g., Li and Kodama, 2016). However, it would also mean that not only the Mengyejing Formation, but also the Denghei

TABLE 3. RESULTS OF THE FOLD TESTS AND REVERSALS TEST AND THE INFERRED ROTATION (R) AND APPARENT LATITUDE DISPLACEMENT (λ) WITH RESPECT TO EURASIA (TORSVIK ET AL., 2012)

		Directions					Fold test			Reversal test of McFadden and McElhinny (1990)	$R \pm \Delta R$		$\lambda \pm \Delta\lambda$	
Formation	Age	N	D (°)	I (°)	α_{95} (°)	k_s/k_g	McElhinny (1964)	McFadden (1990)	Tauxe and Watson (1994) (%)		relative to 30 Ma (°)	relative to 100 Ma (°)	relative to 30 Ma (°)	relative to 100 Ma (°)
E1m	Paleocene	12	36.1	31.5	8.4	27.7/19.1	**Undetermined** (k_s/k_g = 1.45 < F [22, 2]) = 2)	**Undetermined** ($\xi 2_g$ = 9.073, $\xi 2_s$ = 8.211, $\xi_{5\%}$ = 4.036)	52–67		25.2 ± 8.1	23.5 ± 8.1	11.6 ± 7	11.9 ± 7
E2d1	Eocene	12	35.2	35.7	6.5	45.5/23.3	**Undetermined** (k_s/k_g = 1.96 < F [22, 22] = 2)	**Undetermined** ($\xi 2_g$ = 9.729, $\xi 2_s$ = 8.169, $\xi_{5\%}$ = 4.036)	64–78		24.3 ± 6.7	22.6 ± 6.7	8.9 ± 5.5	9.1 ± 5.6
E2d2	Eocene	18	53	33.6	4.3	66.6/29	**Positive** (k_s/k_g = 2.3 > F [34, 34] = 1.77)	**Positive** ($\xi 2_g$ = 12.891, $\xi 2_s$ = 2.969, $\xi_{5\%}$ = 4.940)	72–89		42.1 ± 4.5	40.4 ± 4.6	10.3 ± 3.9	10.5 ± 4
E3m1	Eocene–Oligocene	11	38.4	37.3	9.7	22.9/19.1	**Undetermined** (k_s/k_g = 1.2 < F [20, 20] = 2.12)	**Positive** ($\xi 2_g$ = 6.919, $\xi 2_s$ = 0.405, $\xi_{5\%}$ = 3.865)	60–95		27.5 ± 10	25.8 ± 10	7.8 ± 8	8.1 ± 8
E3m2	Eocene–Oligocene	17	38.6	33	5.7	40/12.1	**Positive** (k_s/k_g = 3.3 > F [32, 32] = 1.8)	**Positive** ($\xi 2g$ = 13.072, $\xi 2_s$ = 2.162, $\xi_{5\%}$ = 4.801)	92–113		27.7 ± 5.7	26 ± 5.8	10.7 ± 4.9	10.9 ± 5
E3m3	Eocene–Oligocene	14	50.8	31.8	5.8	47.7/37.5	**Undetermined** (k_s/k_g = 1.27 < F [26, 26] = 1.93)	**Positive** ($\xi 2_g$ = 5.395, $\xi 2_s$ = 1.425, $\xi_{5\%}$ = 4.358)	87–107		39.9 ± 5.8	38.2 ± 5.8	11.5 ± 5	11.7 ± 5
N1s	Middle Miocene	10	13.5	32.2	5.8	71.2/25.8	**Positive** (k_s/k_g = 2.76 > F [18, 18] = 2.2)	**Positive** ($\xi 2_g$ = 5.478, $\xi 2_s$ = 0.291, $\xi_{5\%}$ = 3.685)	74–92	**Positive** (γ = 9.3° < γ_c = 17.5°, C classification)	2 ± 5.6		12.3 ± 4.8	

Note: D, I, and α_{95}—declination, inclination, and radius of the 95% confidence cone of the formation mean directions in stratigraphical coordinates; k_s/k_g—precision parameter in geographical/stratigraphical coordinates; $R \pm \Delta R$—rotation and its uncertainty; $\lambda \pm \Delta\lambda$—apparent latitude displacement and its uncertainty. $\xi 2g/\xi 2s$—test statistic for the fold test in geographical and stratigraphical coordinates, respectively; ξc—critical value of test statistic for the fold test; $\gamma/\gamma c$—observed angle between the normal and reversal mean directions and critical angle for reversal tests, respectively.

Formation and Mengla Group, would have been deposited in the mid-Cretaceous, which is in serious contradiction with the fossil content of these two formations, because fossil assemblages robustly indicate Eocene to Oligocene ages (YBGMR, 1990). For example, *Sinocypris* in the Denghei Formation is the most abundant ostracod throughout the entire Lower Eocene from East China (He et al., 2011). In addition, Yang et al. (2014) reported volcanics with an age of 36–35 Ma, which overlie the Paleocene Yunlong Formation and, in turn, are overlain by the Baoxiangsi and Lijiang Formations in the northern part of the Lanping-Simao Basin (~250 km north from our studied section). Based on biostratigraphic and lithostratigraphic correlation, the Yunlong Formation is correlative to the Mengyejing Formation, and the Baoxiangsi Formation and Lijiang Formation are correlative to the Denghei Formation and Mengla Group, respectively (YBGMR, 1990). Therefore, even if the Mengyejing Formation were Cretaceous in age, the Denghei Formation and Mengla Group must still be considered Eocene–Oligocene in age. Even if the Mengyejing Formation did contain a primary NRM, the others must be remagnetized given their single polarity. We are then left with the pertinent question: Why would that formation have escaped remagnetization, given that its lithology and magnetic mineralogy are very similar to those of the remagnetized formations?

Next, the microscope results show that the hematites identified in the redbeds are often subhedral to euhedral needles and bundles cementing voids, and rimming quartz and feldspar grains. This clearly indicates that these hematites are secondary.

Further, besides this study, previous paleomagnetic results from Jurassic and Cretaceous sediments in the Jinggu Basin also showed only a single, normal polarity (Huang and Opdyke, 1993; Chen et al., 1995; Gao et al., 2015; Table 4). If all of these normal magnetizations were primary, it would mean that a more than 10-km-thick sediment succession, which is generally considered to span from the Jurassic to the Oligocene, would have been deposited during the ~30 m.y. interval of the Cretaceous normal superchron. This would require a rather high sedimentation rate during the middle Cretaceous, which seems only remotely possible in a relatively tectonic quiet period from a tectonic point of view. In contrast, deposition during the Paleogene in the southeastern margin of the Tibetan Plateau is consistent with the extrusion, folding, and uplift of Indochina caused by the India-Asia collision in the early Cenozoic (Tapponnier et al., 1982; Leloup et al., 1995; Royden et al., 2008; Wang et al., 2012).

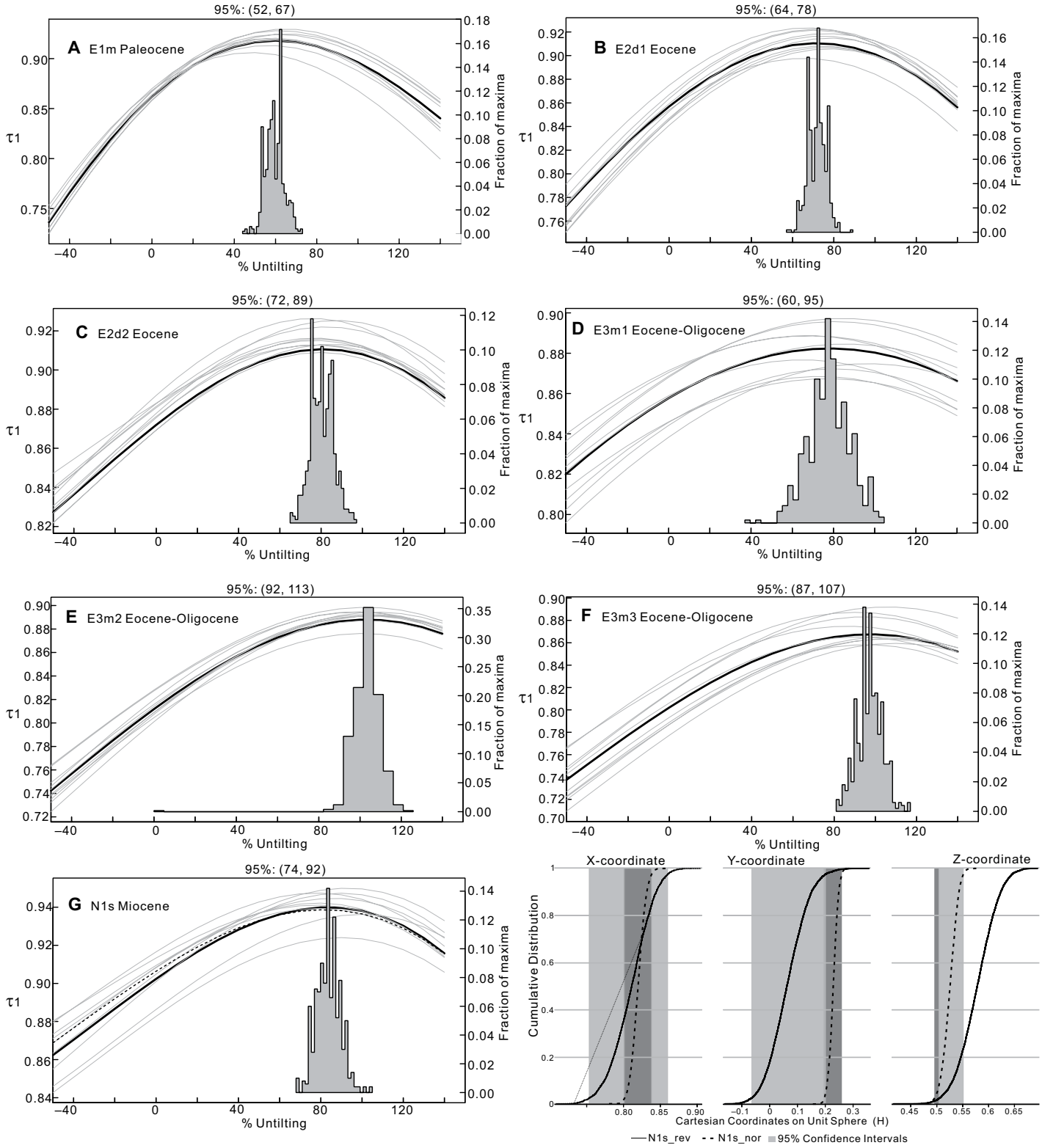

Figure 10. (A–G) Nonparametric fold tests (Tauxe and Watson, 1994) of all the paleomagnetic results and (H) bootstrap reversals test (Tauxe, 2010) on results from the Miocene Sanhaogou Formation. Results of the fold test come with bootstrapped statistics on the first eigenvalues (τ1) upon progressive untilting. The 95% bootstrap error interval is indicated above each panel. Reversed polarity directions for the middle Miocene (G) have been inverted to their antipodes to test a common mean for the normal and reversed magnetization directions. The overlap of 95% confidence intervals for all components indicates a positive reversals test.

TABLE 4. AVAILABLE JURASSIC, CRETACEOUS, AND CENOZOIC PALEOMAGNETIC RESULTS AND CORRESPONDING POLES FROM THE INDOCHINA BLOCK

Location	Latitude (°N)	Longitude (°E)	Age	*N*	Observed direction *D* (°)	Observed direction *I* (°)	Observed direction α_{95} (°)	VGP Latitude (°N)	VGP Longitude (°E)	VGP A_{95} (°)	$R \pm \Delta R$	$\lambda \pm \Delta\lambda$	Possible remagnetization	Present reversal	Test*	Reference
Indochina block																
Khorat Plateau	16.7	101.83	J1	8	37.2	40.1	6.6	54.4	175.6	7.3	34.7 ± 7	15.3 ± 5.3		±	F1	Yang and Besse (1993)
Weishan	25.4	100.2	J1	5	7.3	25.3	10.4	76.3	250	10.4	3.6 ± 9.3	33.4 ± 8.3		+	k_s/k_g = 2.0	Huang and Opdyke (1993)
Khorat Plateau	15.2	105.8	J1	8	35.2	38.9	3.2	56	178.6	2.6	34.6 ± 3.4	14.7 ± 2.6		+		Singsoupho et al. (2014)
Jinggu	23.6	100.5	J2	10	83.3	36.8	5.4	14	173.6	4.2	79.8 ± 5.5	24.4 ± 4.3		+		Huang and Opdyke (1993)
Muang Phin	16.5	106	J1-J2	23	30.8	39.9	3	60.5	178.6	3	30.2 ± 3.2	15.3 ± 2.5		+	Synfolding	Takemoto et al. (2009)
Ratchaburi	13.5	99.7	J1-J2	20	348.5	24.7	10.5	78.6	10.6	9.3	–14.8 ± 9.3	21.8 ± 8.4		±(1site with 3 samples)	F1	Fujiwara et al. (2014)
Nan City	19.2	101	J3-J1	11	32.3	33.3	12.2	60.1	186.5	11.7	20.2 ± 11.7	14.2 ± 9.8		+	F2	Aihara et al. (2007)
Thailand	8.1	99.4	J2-J3	9	31.2	12.2	3.9				19.8 ± 3.2	15.1 ± 3.2		+	F2	Yamashita et al. (2011)
Khorat Plateau	16	102	J3	10	26.6	37.3	2.6	64.8	178.1	2.3	15.1 ± 2.7	8.6 ± 2.2		+		Yang and Besse (1993)
Borikhanxay	18.5	103.8	J3-K1	18	42.1	46.9	7.9	50.7	169.7	8.7	30.8 ± 9.3	4.2 ± 6.3		±	F2/R	Takemoto et al. (2009)
Phong Saly	21.6	101.9	J3-K1	19	28.8	32.1	8.8	63.4	193.9	7.4	16.6 ± 8.3	17.5 ± 7.1		±	F2	Takemoto et al. (2009)
Cambodia	11.6	103.1	J3-K1	11	43.4	31.9	3.6	47.7	178.9	3.6	32.7 ± 3.4	8.1 ± 2.9	Rm?	+		Tsuchiyama et al. (2016)
Khorat Plateau	16.5	102.5	K1	10	32	38.2	4.1	59.4	177.4	4.5	20.4 ± 4.2	–2.7 ± 3.4		+		Yang and Besse (1993)
Khorat Plateau	17	103	K1	4	31.8	38.3	5.7	59.7	178.2	5.7	20.2 ± 5.9	–2.2 ± 4.7		+	F1	Charusiri et al. (2006)
Yunlong	25.8	99.4	K1	23*	59.7	41	11.9	36.2	178.2	11.3	47.2 ± 12.7	3.8 ± 9.6		±	R	Yang et al. (2001)
Yongping	25.5	99.5	K1	12	42	51.1	8.7	50.9	167.3	20.6	29.5 ± 11.2	–4.8 ± 7		+	F1	Funahara et al. (1993)
Jinggu	23.4	100.4	K1	3	84.4	39.6	17.7	13.6	171.5	–	72.1 ± 18.6	2.7 ± 14.2	Rm?	+		Chen et al. (1995)
Jinggu	23.4	100.5	K1	7	115.8	36	6.3	–13.9	161.3	–	103.6 ± 6.3	5.2 ± 5.1		–	F1	Chen et al. (1995)
Jinggu	23.5	100.4	K1	47	77	43	2.9				64.7 ± 3.3	0.3 ± 2.5		+	F1\F2	Gao et al. (2015)
Menglun	21.9	101.2	K1	19	46.2	45.9	10.6	48.9	172.9	12.6	34.1 ± 12.3	–3.5 ± 8.5		±	F1\F2	Tong et al. (2013)
Mengla	21.4	101.6	K1	14	46.9	42.2	7.7	45.3	177.2	8.5	34.9 ± 8.4	–1 ± 6.2		+	F1\F2	Tong et al. (2013)
Khorat Plateau	18.1	102.4	K1	10	25.9	37.4	10.2	65.1	171.5	12.6	14.2 ± 10.3	–0.6 ± 8.2		±	F	Singsoupho et al. (2014)
Khorat Plateau	16.7	105.4	K1	8	28.8	45.7	5	61.2	168.7	5.2	17.3 ± 5.8	–7.6 ± 4.1		+	F	Singsoupho et al. (2014)
Khorat Plateau	18.3	103.4	K2	16	21.2	37.1	7.7	69.9	181.5	8.2	6.3 ± 7.9	6.8 ± 6.4		+	F	Singsoupho et al. (2014)
Khorat Plateau	16.5	105.5	K2	12	27.7	38	4.1	63.3	180	3.9	13.4 ± 4.4	5 ± 3.7		+	F	Singsoupho et al. (2014)
Song Da	21	104.4	K2	8	3.2	26.7	12.9	83.2	255.6	10.8	–11.9 ± 11.7	16.3 ± 10.4		±	F1\R	Takemoto et al. (2005)
Song Da	22.3	103.4	K2	5	12.2	40.1	4.7	78.7	188	5.1	–3.3 ± 5.1	8.6 ± 4		+	F1\F2	Takemoto et al. (2005)
Khorat Plateau	17.5	103.5	K2	14	31.8	28.7	3.5	59.4	190.8	3.5	17 ± 3.5	11.5 ± 3.2		+	k_s/k_g = 1.01	Charusiri et al. (2006)
Khorat Plateau	17	103	K2	8	31.4	27.1	9.4	59.7	192.7	9.4	16.6 ± 8.6	11.8 ± 7.7		+	k_s/k_g = 1.1	Charusiri et al. (2006)
Yunlong	25.8	99.4	K2	9	34	52.4	7.3	69.7	167.6	7.3	17.3 ± 9.7	0.7 ± 6		+	F1\F2	Yang et al. (2001)
Yunlong	25.8	99.4	K2	20	40.2	49.9	3.5	54.6	171.8	4.4	23.5 ± 4.6	3 ± 3.1		+	F1\F2	Sato et al. (1999)
Xiaguan	25.6	100.2	K2	9	6.9	47.7	8.6	83.6	152.7	10	–9.7 ± 10.4	5 ± 7		±	F1\R	Huang and Opdyke (1993)
Jingdong	24.5	100.8	K2	13	8.3	48.3	7.7	81.2	145.8	8.9	–8 ± 9.4	3.6 ± 6.3		+	F2	Tanaka et al. (2008)
Zhenyuan	24	101.1	K2	7	61.8	46.1	8.1	34.7	172.7	8.1	45.7 ± 9.5	5 ± 6.6		+	F2	Tanaka et al. (2008)
West Zhenyuan	24	101.1	K2	4	144.2	49.4	6.4	-25.7	135.2	7.7	128.1 ± 8	2.2 ± 5.3		–	F2	Tanaka et al. (2008)
Jinggu	23.4	100.9	K2	8	79.4	43.3	9.1	18.9	170	8.9	63.4 ± 10.2	6.6 ± 7.4		+	k_s/k_g = 1.8	Huang and Opdyke (1993)
Mengla	21.6	101.4	K2	10	60.8	37.8	7.6	33.7	179.3	8.2	45.1 ± 7.8	9 ± 6.3		±(1site)		Huang and Opdyke (1993)
Zhengwan	22.8	100.9	K2	11	51.8	47.9	6.9	42.4	170.1	7.8	35.9 ± 8.4	2.3 ± 5.7		±	F/R	Kondo et al. (2012)
Daduanggang	22.4	101	K2	12	64.1	48.1	7.3	32.3	169	8.6	48.2 ± 8.9	1.8 ± 6		+	F2	Kondo et al. (2012)

(*continued*)

TABLE 4. AVAILABLE JURASSIC, CRETACEOUS, AND CENOZOIC PALEOMAGNETIC RESULTS AND CORRESPONDING POLES FROM THE INDOCHINA BLOCK (*continued*)

Location	Latitude (°N)	Longitude (°E)	Age	*N*	Observed direction *D* (°)	*I* (°)	α_{95} (°)	VGP Latitude (°N)	VGP Longitude (°E)	A_{95} (°)	$R \pm \Delta R$	$\lambda \pm \Delta\lambda$	Possible remagnetization	Present reversal	Test*	Reference
Menglun	21.9	101.2	K2	6	33.2	30.9	8.2	56.3	195.8	8.2	17.4 ± 7.8	13.8 ± 6.7		+	F1	Tong et al. (2013)
Da Lat	11.7	108.3	K2	21	11.4	35.4	1.7	76.5	161.2	1.7	–1.9 ± 2.2	2.7 ± 2.2		+	F2	Otofuji et al. (2012)
Mengban	21.8	101.6	K1–2	4	50.5	31	6.4	42.2	188.5	6.8	34.8 ± 6.2	13.7 ± 5.3		+	F1\F2	Tong et al. (2013)
Puer	23	101	K	25	59.9	45.2	5.1	35.8	173.1	5.6	43.9 ± 6	4.7 ± 4.3		+	F1\F2	Sato et al. (2007)
South Mengla	21.4	101.6	K	13	51.2	46.4	5.6	43.6	172.1	6.1	35.6 ± 6.7	2.4 ± 4.7		±(2samples)	F2	Tanaka et al. (2008)
Da Lat	11	108	K	21	14.5	33.3	6.3	74.2	171.1	5.9	1.2 ± 6.2	3.3 ± 5.4		+	k_s/k_g = 1.0	Chi and Dorobek (2004)
Yunlong	25.8	99.4	P	11*	50.2	31.1	13.2				38.2 ± 12.4	12.2 ± 10.6		±	R	Yang et al. (2001)
Jinggu	23.5	100.7	P	35*	42.8	26.1	7.9	48.5	196.4	–	31.2 ± 7.1	13.3 ± 6.4	Rm?	+		Chen et al. (1995)
Mengban	21.8	101.6	P	6	43.5	23	13.4	46.4	196.7	12.2	32.1 ± 11.7	13.5 ± 10.8		±		Tong et al. (2013)
Lanping-Simao	26.5	99.3	E	9	86.1	39.8	11.2	14.5	169.7	10.9	74.6 ± 12.1	7.6 ± 9.4		–	F2	Sato et al. (2001)
Mengla	21.5	101.7	E	11	51.7	33.4	8.7	41.3	185.2	8.5	40.8 ± 8.8	7.5 ± 7.6		±	F1\F2\R	Yang and Otofuji (2001)
Jinggu	23.5	100.8	E	6	73.1	39.9	11.8	23.2	174.6	12.2	62 ± 12.7	4.8 ± 9.9		+		Yang and Otofuji (2001)
Jinggu	23.5	100.7	E-O	32*	84.7	38.9	7.6	13.2	209.2	–	73.6 ± 8.3	5.5 ± 6.8	Rm?	+		Chen et al. (1995)
Mengla	21.5	101.5	O	17	41.8	23.8	5.8	48.4	194.8	5.8	31.1 ± 5.4	14.4 ± 5		+	F1	Tong et al. (2013)
Jinggu	23.5	100.7	O(P)	12	36.1	31.5	8.4	55.7	194.5	8.5	25.2 ± 8.1	11.6 ± 7	Rm	+		This Study
Jinggu	23.5	100.7	O(E2d1)	12	35.2	35.7	6.5	57.2	189.6	5.7	24.3 ± 6.7	8.9 ± 5.5	Rm	+		This Study
Jinggu	23.5	100.7	O(E2d2)	18	53	33.6	4.3	40.5	186	4.3	42.1 ± 4.5	10.3 ± 3.9	Rm	+	F1\F2	This Study
Jinggu	23.5	100.7	O(E3m1)	11	38.4	37.3	9.7	54.8	186.2	9.4	27.5 ± 10	7.8 ± 8	Rm	+	F2	This Study
Jinggu	23.5	100.7	O(E3m2)	17	38.6	33	5.7	53.9	191.8	5.1	27.7 ± 5.7	10.7 ± 4.9	Rm	+	F1\F2	This Study
Jinggu	23.5	100.7	O(E3m3)	14	50.8	31.8	5.8	43.1	187.9	5.2	39.9 ± 5.8	11.5 ± 5	Rm	+	F2	This Study
Puer	23	101	O?(T2)	18	95.4	28.4	6.2	0.9	174.3	5.2	84.5 ± 5.9	13.1 ± 5.3	Rm	+		Huang and Opdyke (2015)
Jinggu	23.5	100.7	M	29*	21.1	35.5	7.1	70	197.8	–	9.6 ± 7.1	10.1 ± 5.8		±		Chen et al. (1995)
Mae Moh	18.3	99.7	M	86*	358.3	22.2	4				–12.8 ± 3.6	12.9 ± 3.4		±	R	Benammi et al. (2002)
Mae Moh	18.3	99.7	M	65*	5.4	26.5	7.1				–5.7 ± 6.4	10.5 ± 5.8		±	R	Coster et al. (2010)
Chiang Muan	18	100	M	21*	5.7	33.6	10.3				–5.3 ± 10	5.8 ± 8.3		±	R	Benammi et al. (2004)
Jinggu	23.5	100.4	M	38*	13.7	36	3.3				2.2 ± 3.4	9.7 ± 2.9		±		Gao et al. (2015)
Jinggu	23.5	100.7	M	10	13.5	32.2	5.8	77	214.9	5.5	2 ± 5.6	12.3 ± 4.8			F1\F2\R	This Study
Eurasia			J1	180 Ma				68.5	107.2	0.7						Torsvik et al. (2012)
			J2-J3	160 Ma				72.9	138	0.6						
			K1	120 Ma				78.7	179	0.8						
			K2	80 Ma				73.5	156.7	1.6						
			P	60 Ma				78.9	169.8	1.2						
			E	40 Ma				79.2	166.6	3.1						
			E-O	30 Ma				78.9	160.6	2						
			M	20 Ma				78	156.9	1.2						

Note: Age—age range of sampled rocks (J1—Early Jurassic; J2—Middle Jurassic; J3—Late Jurassic; K1—Early Cretaceous; K2—Late Cretaceous; P—Paleocene; E—Eocene; O—Oligocene; M—Miocene); *N*—number of sites or specimens (*). Observed direction: D—declination, I—inclination, α_{95}—radius of 95% confidence level. VGP—virtual geomagnetic pole, giving latitude, longitude, and radius of 95% confidence circle (A_{95}) of mean observed VGP. Rotational (*R*) and apparent latitudinal displacement (λ) were evaluated by comparing the observed paleomagnetic declinations with those expected from the Eurasian paleomagnetic poles (Torsvik et al., 2012). Uncertainties in rotation (ΔR) and apparent latitudinal displacement ($\Delta\lambda$) were calculated using methods described in Butler (1992). Rm—remagnetization or possible remagnetization (Rm?) as claimed by the original authors; ± indicates normal and reversal polarity present in the paleomagnetic data.

*Test, fold, and reversals test: F1—fold test of McElhinny (1964); F2—fold test of McFadden (1990); R—reversals test of McFadden and McElhinny (1990); k_s/k_g —ratio of changes in precision parameter (Fisher, 1953) for inconclusive fold test, where k_g and k_s are the values in geographical and stratigraphical coordinates, respectively.

Finally, large-scale remagnetization in the southeastern Tibetan Plateau was recognized in recent studies (Liu et al., 2011; Yamashita et al., 2011; Appel et al., 2012; Kornfeld et al., 2014a; Huang and Opdyke, 2015; Tong et al., 2016; Tsuchiyama et al., 2016; for locations, see Fig. 1A). The rocks investigated include metamorphic rocks (Appel et al., 2012), metabasalts (Kornfeld et al., 2014a), limestones (Huang and Opdyke, 2015), and redbeds (Liu et al., 2011; Yamashita et al., 2011; Huang and Opdyke, 2015; Tong et al., 2016; Tsuchiyama et al., 2016), with ages ranging from Permian to Oligocene. The remagnetization was suggested to have occurred either during the early Cenozoic or during the Eocene–Oligocene.

Therefore, the normal paleomagnetic directions isolated from the Paleogene redbeds in the Jinggu Basin are most likely remagnetized. In this case, the flattening of the inclinations with respect to Eurasia may be the result of nonrigid behavior of Eurasia and/or inaccuracies in the Eurasian apparent polar wander path (APWP) in Paleogene time. Paleomagnetic inclinations from Mesozoic and Cenozoic sediments of East Asia are systematically 10°–20° lower than the Eurasian APWP would imply (e.g., Li et al., 2013). This is often interpreted as being related to inclination shallowing of sediments. However, recent paleolatitudes determined from Oligocene effusive rocks of northern East Asia, devoid of inclination shallowing, are still 5°–10° lower than expected (e.g., Dupont-Nivet et al., 2010b), suggesting that either East Asia was located more to the south, implying that Eurasia is not a rigid block (Cogné et al., 2013), or that the Eurasian APWP in Paleogene time is imperfect. It should be realized much of the Eurasian APWP data derive from Europe and have been recalculated to locations in Asia under the assumption of Eurasia being a rigid block.

Age and Possible Mechanism for the Acquisition of the Remagnetization

If the ChRMs resolved from the Mengyejing Formation, the Denghei Formation, and the Mengla Group are remagnetized, the remagnetization must have been acquired sometime after the late Eocene–early Oligocene deposition of the Mengla Group and before the unremagnetized Miocene. In addition, the positive fold tests show that the magnetization was acquired before folding, whereby folding of the youngest Mengla Group occurred in the late Oligocene (YBGMR, 1990; He et al., 1996), suggesting an Oligocene age of remagnetization.

Remagnetization is frequently found in sedimentary rocks (e.g., Kent et al., 1987; Geissman and Harlan, 2002; Huang et al., 2015a, 2015b). It can be caused either by thermoviscous resetting (e.g., Kent, 1985) or chemical remanent magnetization (CRM) acquired during diagenesis or incipient metamorphism (Geissman and Harlan, 2002; Liu et al., 2011; Dekkers, 2012; Elmore et al., 2012; Huang et al., 2015a, 2015b). A thermoviscous remagnetization for the Paleogene redbeds in Jinggu Basin can be ruled out because of the absence of any documented magmatism of Cenozoic age in the Jinggu Basin. The polished thin section study indicates that the sediments did not undergo significant metamorphism. Therefore, a CRM residing in secondary hematite is the most plausible mechanism for the remagnetization. In fact, widespread remagnetization events linked to CRM acquisition by low-temperature fluid alteration have been described worldwide, especially in North America (e.g., McCabe and Elmore, 1989; Elmore et al., 1993; Geissman and Harlan, 2002) and East Asia (e.g., Kent et al., 1987; Liu et al., 2011; Appel et al., 2012; Huang et al., 2015a, 2015b). Based on a detailed rock magnetic, petrographic, and X-ray diffraction study of the Triassic Feixianguan Formation redbeds in Zhaotong (~500 km northeast from the Jinggu Basin), northeast Yunnan, Liu et al. (2011) proposed that the remagnetization of the Feixianguan redbeds was due to fluid migration, which mobilized iron from silicate coatings and precipitated it almost instantaneously as (pigmentary) hematite. This mechanism was employed by Huang and Opdyke (2015) to interpret the remagnetization of Dashuijingshan limestones in Pu'er (~60 km southeast from the Jinggu Basin), southern Yunnan Province. The growth of hematite along cracks or around edges of quartz grains shown by the SEM in our study concurs with the hypothesis of Liu et al. (2011), i.e., secondary hematite growth induced by migrating fluids in our Paleogene redbeds. In that context, it is interesting to note that there are widespread hydrothermal mineralizations of early Oligocene age within the southeast margin of the Tibetan Plateau (Deng et al., 2014) and also in the Jinggu Basin itself, which demonstrate that fluid activity was omnipresent in the study area in the time interval of remagnetization. Exhumation and uplift of the southeast margin of the Tibetan Plateau and the onset of extrusion of Indochina along the Ailao Shan–Red River fault and the Shan scarp also occurred in the Oligocene (Tapponnier et al., 1982; Bertrand et al., 2001; Schoenbohm et al., 2005; Zhou et al., 2007). We, therefore, suggest that these tectonic processes changed the hydraulic head, which would have induced fluid migration. The porous and well-sorted structure of Paleogene sandstones provides efficient pathways for fluids, which resulted in remagnetization of the Paleogene redbeds in the Jinggu Basin.

Tectonic Implications for the Clockwise Rotations of the Indochina Block

Although we prefer remagnetization as the most reasonable interpretation of the paleomagnetic results from the redbeds, we considered both an Oligocene (if remagnetized) and a ca. 110–100 Ma age (if primary) of magnetization to assess whether the two ages would yield very different tectonic interpretations. Therefore, to evaluate the magnitude of rotation and latitudinal displacement of the Indochina block, both the 100 Ma and 30 Ma poles on the APWP of Eurasia (Torsvik et al., 2012) were used as a reference pole for the redbeds, and the 20 Ma pole from the APWP was used for the middle Miocene. The amount of rotation (R) and displacement (λ) were calculated following Butler (1992) as $R = D_{obs} - D_{exp}$, and $\lambda = \lambda_{exp} - \lambda_{obs}$, where D_{obs} and λ_{obs} are the observed declination and paleolatitude, respectively, and D_{exp} and λ_{exp} are the expected declination and paleolatitude derived from the reference pole, respectively. Their uncertainties, ΔR and $\Delta\lambda$, are also given by Butler (1992).

When compared to the expected direction derived from the reference pole, the paleomagnetic declinations from our redbeds yield a clockwise rotation of ~25°–42° with respect to Eurasia no matter which age of the pole was used, i.e., 30 or 100 Ma (Fig. 11; Table 3), while the middle Miocene declination suggests 2° ± 5.6° clockwise rotation with respect to Eurasia since the middle Miocene (Table 3). In terms of latitudinal displacement, the paleomagnetic inclinations from redbeds imply that the studied area experienced a ~8°–12° northward motion with respect to Eurasia since the middle Cretaceous or Oligocene (Table 3). The middle Miocene inclination suggests a similar northward motion of 12.3° ± 4.8° with respect to Eurasia since the middle Miocene (Table 3), which is in contrast with the southward motion of Indochina as suggested by the extrusion model.

When comparing the amount of rotation and latitudinal displacement with previous results from the Indochina block (e.g., Yang and Besse, 1993; Yang et al., 1995, 2001; Sato et al., 2007; Chi and Geissman, 2013; Tong et al., 2013, 2015; Gao et al., 2015), this analysis clearly shows that the ~30°–40° clockwise rotation suggested by the directions from redbeds is in good agreement with most of the previous Mesozoic and early Cenozoic paleomagnetic results (Fig. 11A). The smaller clockwise rotation inferred by the middle Miocene direction is also consistent with other Miocene results (Fig. 11A). This suggests that no significant rotation has occurred within the Indochina block during Late Cretaceous to Eocene times, and most of the clockwise rotation

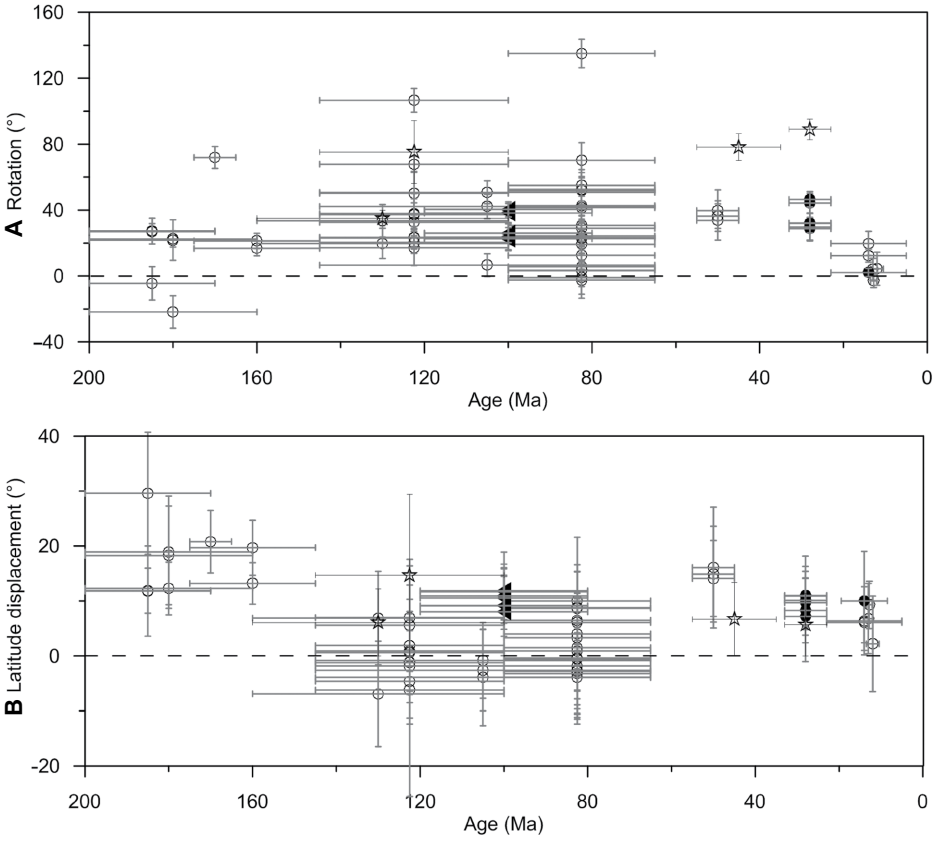

Figure 11. Observed rotations and apparent latitudinal displacement from currently available paleomagnetic results of the Indochina block relative to Eurasia (Torsvik et al., 2012) as a function of age. Vertical and horizontal lines represent 95% confidence intervals in rotation/displacement and uncertainties in age or age span (see Table 4), respectively. The precision of the age constraints varies with age errors spanning an entire period (e.g., Cretaceous [145–65 Ma] become 105.5 ± 40.5 Ma) or from magnetostratigraphy results (e.g., 12.8 ± 0.7 Ma of the Mae Moh Basin spanning from 13.5 to 12.1 Ma; Benammi et al., 2002). The open circles represent the "primary" directions. The solid dots and stars denote results of this study and previous remagnetized directions, respectively. The triangles represent the directions from redbeds of this study when interpreted as being primary from the Cretaceous. See Table 4 for more detailed information.

of Indochina occurred between the Oligocene and middle Miocene, i.e., when the Ailao Shan–Red River fault and the Shan scarp were active (Leloup et al., 1995). After the middle Miocene, the amount and rate of rotation decreased rather substantially (Fig. 11A). The rapid rotation of the Indochina block between the Oligocene and middle Miocene, followed by slower rotation in more recent times, is in accordance with the rotation pattern of the Tengchong block (Kornfeld et al., 2014b), which suggests that the two blocks may share a similar deformation mechanism in the Cenozoic.

Besides the large block rotation detected by paleomagnetic data, we also find some local rotations in the Jinggu Basin. For example, sites m8–m13 were collected close to a fault (Fig. 1B), and the tilt-corrected mean paleomagnetic direction from these five sites (site m9 was discarded because of large α95; Table 1) is D = 87.6°, I = 37.3°, α_{95} = 4.4°, which suggests an ~80° clockwise rotation in this area. In fact, more than 60° clockwise rotation was also reported by previous paleomagnetic studies (Huang and Opdyke, 1993; Chen et al., 1995; Sato et al., 2001; Tanaka et al., 2008; Huang and Opdyke, 2015; Gao et al., 2015). These large clockwise rotations most likely reflect superimposed local rotation on regional block rotation.

Only a few individual inclination results indicate minor southward motion of the Indochina block (Fig. 11B; Table 4). In contrast, most results, including the paleomagnetic results from this study, suggest an ~10° northward motion of the Indochina block with respect to Eurasia (Fig. 11B; Table 4). A northward motion of the Indochina block since the Cretaceous is, however, not likely given the tectonic history of the region. Plausible reasons for this "anomaly" include widespread inclination shallowing of sediments (e.g., Li and Kodama, 2016), or inaccuracies in the relocation of the Eurasian APWP to sites in East Asia (Dupont-Nivet et al., 2010b).

Many previous paleomagnetic studies in Indochina have been undertaken on redbeds from the Jurassic to early Cenozoic. Most of those results show exclusive normal polarity; author groups, however, took a positive fold test as the main argument for a primary magnetization (Table 4). However, the age of these redbeds is not always well constrained. Therefore, whether these paleomagnetic results indeed record a primary magnetization or a remagnetization remains a subject that is difficult to resolve. If the magnetization isolated from the redbeds in the present study is primary, the age of the sediments in the Indochina block should be thoroughly reexamined. However, if the magnetization isolated from the redbeds in this study is a remagnetization, the remagnetization in the Indochina block may be more widespread than previously appreciated. To address this issue, additional detailed paleomagnetic and rock-magnetic studies, coming with well-defined sediment ages, are required.

CONCLUSIONS

In this study, we identified a prefolding magnetization, but with an exclusively normal polarity, from a 3-km-thick sequence of redbeds from the Jinggu Basin, Indochina block. Biostratigraphic results indicate that the redbeds have a Paleogene age, which would imply a regional remagnetization. An alternative interpretation based on U/Pb ages of tuffs found in the lowermost Mengyejing Formation in the Jiangcheng Basin could indicate a primary magnetization acquired in the Cretaceous normal superchron. The remagnetization hypothesis is supported by rock magnetic and microscopy results and is much more consistent with the regional geological setting, and therefore it is our preferred interpretation. Paleomagnetic results from middle Miocene rocks pass both fold and reversals tests and thus represent primary magnetizations. The easterly deflected declination isolated from the redbeds indicates that the Jinggu Basin has been subject to ~30°–35° of clockwise rotation with respect to Eurasia since the Late Cretaceous (if primary) or Oligocene (if remagnetized), while the middle Miocene paleomagnetic result indicates insignificant clockwise rotation, which suggests that the Jinggu Basin experienced a rapid clockwise rotation between the Oligocene and middle Miocene, when the Ailao Shan–Red

River fault and Shan scarp were active, but much slower rotation during more recent times. Considering that the ages of many Jurassic–Paleogene redbeds targeted in several earlier paleomagnetic studies are rather ambiguous, the dispute between the primary magnetization and remagnetization cannot be fully resolved yet. Hence, interpretation of paleomagnetic data for tectonic purposes must be done with caution; improved age control is essential for a more robust interpretation.

ACKNOWLEDGMENTS

We thank Cor Langereis for helpful discussions and Saihong Yang for assistance during scanning electron microscope measurement. Associate Editor M. Mattei, F. Speranza, and an anonymous reviewer are appreciated for their constructive reviews. Brad S. Singer is thanked for his editing of this paper. Financial assistance was provided by the National Natural Science Foundation of China grant 41404056 and the State Key Laboratory of Lithospheric Evolution grant 11431780. S. Li acknowledges further support from the China Postdoctoral Science Foundation grant 127803, and van Hinsbergen was funded through ERC (European Research Council) Starting Grant 306810 (SINK) and NWO (Netherlands Organization for Scientific Research) VIDI grant 864.11.004.

REFERENCES CITED

Aihara, K., Takemoto, K., Zaman, H., Inokuchi, H., Miura, D., Surinkum, A., Paiyarom, A., Phajuy, B., Chantraprasert, S., Panjasawatwong, Y., Wongpornchai, P., and Otofuji, Y., 2007, Internal deformation of the Shan-Thai block inferred from paleomagnetism of Jurassic sedimentary rocks in northern Thailand: Journal of Asian Earth Sciences, v. 30, no. 3–4, p. 530–541, doi:10.1016/j.jseaes.2007.01.002.

Appel, E., Crouzet, C., and Schill, E., 2012, Pyrrhotite remagnetizations in the Himalaya: A review, *in* Elmore, R.D., Muxworthy, A.R., Aldana, M.M., and Mena, M., eds., Remagnetization and Chemical Alteration of Sedimentary Rocks: Geological Society, London, Special Publication 371, p. 163–180, doi:10.1144/SP371.1.

Benammi, M., Urrutia-Fucugauchi, J., Alva-Valdivia, L.M., Chaimanee, Y., Triamwichanon, S., and Jaeger, J.J., 2002, Magnetostratigraphy of the middle Miocene continental sedimentary sequences of the Mae Moh Basin in northern Thailand: Evidence for counterclockwise block rotation: Earth and Planetary Science Letters, v. 204, no. 3–4, p. 373–383, doi:10.1016/S0012-821X(02)01002-6.

Benammi, M., Chaimanee, Y., Urrutia-Fucugauchi, J., and Jaeger, J.-J., 2004, Magnetostratigraphic study of the continental sedimentary sequence of the Chiang Muan Basin, northern Thailand: Implications for the age of the first Miocene hominoids from Thailand: International Geology Review, v. 46, no. 7, p. 646–654, doi:10.2747/0020-6814.46.7.646.

Bertrand, G., Rangin, C., Maluski, H., Bellon, H., and GIAC Scientific Party, 2001, Diachronous cooling along the Mogok metamorphic belt (Shan scarp, Myanmar): The trace of the northward migration of the Indian syntaxis: Journal of Asian Earth Sciences, v. 19, p. 649–659, doi:10.1016/S1367-9120(00)00061-4.

Briais, A., Patriat, P., and Tapponnier, P., 1993, Updated interpretation of magnetic anomalies and seafloor spreading stages in the South China Sea: Implications for the Tertiary tectonics of Southeast Asia: Journal of Geophysical Research, v. 98, no. B4, p. 6299–6328, doi:10.1029/92JB02280.

Butler, R.F., 1992, Paleomagnetism: Magnetic Domains to Geologic Terranes: Oxford, UK, Blackwell Scientific Publications, 319 p.

Charusiri, P., Imsamut, S., Zhuang, Z.H., Ampaiwan, T., and Xu, X.X., 2006, Paleomagnetism of the earliest Cretaceous to early Late Cretaceous sandstones, Khorat Group, northeast Thailand: Implications for tectonic plate movement of the Indochina block: Gondwana Research, v. 9, no. 3, p. 310–325, doi:10.1016/j.gr.2005.11.006.

Chen, H.H., Dobson, J., Heller, F., and Hao, J., 1995, Paleomagnetic evidence for clockwise rotation of the Simao region since the Cretaceous: A consequence of India-Asia collision: Earth and Planetary Science Letters, v. 134, p. 203–217, doi:10.1016/0012-821X(95)00118-V.

Chi, C.T., and Dorobek, S.L., 2004, Cretaceous paleomagnetism of Indochina and surrounding regions: Cenozoic tectonic implications, *in* Malpas, J., Fletcher, C.J.N., Ali, J.R., and Aitchison, J.C., eds., Aspects of the Tectonic Evolution of China: Geological Society, London, Special Publication 226, p. 273–287.

Chi, C.T., and Geissman, J.W., 2013, A review of the paleomagnetic data from Cretaceous to Lower Tertiary rocks from Vietnam, Indochina and South China, and their implications for Cenozoic tectonism in Vietnam and adjacent areas: Journal of Geodynamics, v. 69, p. 54–64, doi:10.1016/j.jog.2011.11.008.

Cogné, J.P., Besse, J., Chen, Y., and Hankard, F., 2013, A new Late Cretaceous to Present APWP for Asia and its implications for paleomagnetic shallow inclinations in Central Asia and Cenozoic Eurasian plate deformation: Geophysical Journal International, v. 192, no. 3, p. 1000–1024, doi:10.1093/gji/ggs104.

Coster, P., Benammi, M., Chaimanee, Y., Yamee, C., Chavasseau, O., Emonet, E.G., and Jaeger, J.J., 2010, A complete magnetic-polarity stratigraphy of the Miocene continental deposits of Mae Moh Basin, northern Thailand, and a reassessment of the age of hominoid-bearing localities in northern Thailand: Geological Society of America Bulletin, v. 122, no. 7–8, p. 1180–1191, doi:10.1130/B26568.1.

Creer, K.M., 1962, The dispersion of the geomagnetic field due to secular variation and its determination for remote times from paleomagnetic data: Journal of Geophysical Research, v. 67, p. 3461–3476, doi:10.1029/JZ067i009p03461.

Curray, J.R., 2005, Tectonics and history of the Andaman Sea region: Journal of Asian Earth Sciences, v. 25, no. 1, p. 187–232, doi:10.1016/j.jseaes.2004.09.001.

Deenen, M., Langereis, C.G., van Hinsbergen, D.J.J., and Biggin, A., 2011, Geomagnetic secular variation and the statistics of paleomagnetic directions: Geophysical Journal International, v. 186, p. 509–520, doi:10.1111/j.1365-246X.2011.05050.x.

Dekkers, M.J., 2012, End-member modelling as an aid to diagnose remagnetization: A brief review, *in* Elmore, R.D., Muxworthy, A.R., Aldana, M.M., and Mena, M., eds., Remagnetization and Chemical Alteration of Sedimentary Rocks: Geological Society, London, Special Publication 371, p. 253–269, doi:10.1144/SP371.12.

Deng, J., Wang, Q., Li, G., and Santosh, M., 2014, Cenozoic tectono-magmatic and metallogenic processes in the Sanjiang region, southwestern China: Earth-Science Reviews, v. 138, p. 268–299, doi:10.1016/j.earscirev.2014.05.015.

Dupont-Nivet, G., Lippert, P.C., van Hinsbergen, D.J.J., Meijers, M.J.M., and Kapp, P., 2010a, Palaeolatitude and age of the Indo-Asia collision: Palaeomagnetic constraints: Geophysical Journal International, v. 182, p. 1189–1198, doi:10.1111/j.1365-246X.2010.04697.x.

Dupont-Nivet, G., van Hinsbergen, D.J.J., and Torsvik, T.H., 2010b, Persistently low Asian paleolatitudes: Implications for the India-Asia collision history: Tectonics, v. 29, no. 5, TC5016, doi:10.1029/2008TC002437.

Elmore, R.D., London, D., Bagley, D., Fruit, D., and Gao, G., 1993, Remagnetization by basinal fluids: Testing the hypothesis in the Viola limestone, southern Oklahoma: Journal of Geophysical Research, v. 98, p. 6237–6254, doi:10.1029/92JB02577.

Elmore, R.D., Muxworthy, A.R., and Aldana, M., 2012, Remagnetization and chemical alteration of sedimentary rocks, *in* Elmore, R.D., Muxworthy, A.R., Aldana, M.M., and Mena, M., eds., Remagnetization and Chemical Alteration of Sedimentary Rocks: Geological Society, London, Special Publication 371, p. 1–21, doi:10.1144/SP371.15.

Fisher, R., 1953, Dispersion on a sphere: Proceedings of the Royal Society of London, ser. A, Mathematical and Physical Sciences, v. 217, p. 295–305, doi:10.1098/rspa.1953.0064.

Fujiwara, K.P., Zaman, H., Surinkum, A., Chaiwong, N., Fujihara, M., Ahn, H.-S., and Otofuji, Y.-I., 2014, New insights into regional tectonics of the Indochina Peninsula inferred from Lower-Middle Jurassic paleomagnetic data of the Sibumasu terrane: Journal of Asian Earth Sciences, v. 94, p. 126–138, doi:10.1016/j.jseaes.2014.08.020.

Funahara, S., Nishiwaki, N., Murata, F., Otofuji, Y., and Wang, Y.Z., 1993, Clockwise rotation of the Red River fault inferred from paleomagnetic study of Cretaceous rocks in the Shan-Thai-Malay block of western Yunnan, China: Earth and Planetary Science Letters, v. 117, no. 1–2, p. 29–42, doi:10.1016/0012-821X(93)90115-P.

Gao, L., Yang, Z., Tong, Y., Wang, H., and An, C., 2015, New paleomagnetic studies of Cretaceous and Miocene rocks from Jinggu, western Yunnan, China: Evidence for internal deformation of the Lanping-Simao terrane: Journal of Geodynamics, v. 89, p. 39–59, doi:10.1016/j.jog.2015.06.004.

Geissman, J., and Harlan, S.S., 2002, Late Paleozoic remagnetization of Precambrian crystalline rocks along the Precambrian/Carboniferous nonconformity, Rocky Mountains: A relationship among deformation, remagnetization, and fluid migration: Earth and Planetary Science Letters, v. 203, p. 905–924, doi:10.1016/S0012-821X(02)00932-9.

Gilley, L., 2003, Direct dating of left-lateral deformation along the Red River shear zone, China and Vietnam: Journal of Geophysical Research, v. 108, no. B2, 2127, doi:10.1029/2001JB001726.

Hall, R., van Hattum, M.W.A., and Spakman, W., 2008, Impact of India-Asia collision on SE Asia: The record in Borneo: Tectonophysics, v. 451, no. 1–4, p. 366–389, doi:10.1016/j.tecto.2007.11.058.

He, J., van Nieuwenhuise, D.S., and Swain, F.M., 2011, Biostratigraphy of Paleogene non-marine ostracode from East China, *in* Hanai, T., Ikeya, N., and Ishizaki, K., ed., Evolutionary of Biology of Ostracoda: Its Fundamentals and Applications: Amsterdam, Elsevier, p. 1153–1162.

He, K., He, H., and Cai, H., 1996, Formation and evolution of the western Yunnan orogenic belt: Geological Review, v. 42, no. 2, p. 97–106.

Hu, X., Garzanti, E., Moore, T., and Raffi, I., 2015, Direct stratigraphic dating of India-Asia collision onset at the Selandian (middle Paleocene, 59 ± 1 Ma): Geology, v. 43, p. 859–862, doi:10.1130/G36872.1.

Huang, K., and Opdyke, N.D., 1993, Paleomagnetic results from Cretaceous and Jurassic rocks of south and southwest Yunnan—Evidence for large clockwise rotations in the Indo-China and Shan Thai Malay terranes: Earth and Planetary Science Letters, v. 117, p. 507–524, doi:10.1016/0012-821X(93)90100-N.

Huang, K., and Opdyke, N.D., 2015, Post-folding magnetization of the Triassic rocks from western Guizhou and southern Yunnan Provinces: New evidence for large clockwise rotations in the Simao terrane: Earth and Planetary Science Letters, v. 423, p. 155–163, doi:10.1016/j.epsl.2015.05.015.

Huang, W., Dupont-Nivet, G., Lippert, P.C., Hinsbergen, D.J.J.v., Dekkers, M.J., Guo, Z., Waldrip, R., Li, X., Zhang, X., Liu, D., and Kapp, P., 2015a, Can a primary remanence be retrieved from partially remagnetized Eocene volcanic rocks in the Nanmulin Basin (southern Tibet) to date the India-Asia collision?: Journal of Geophysical Research, v. 120, p. 42–66, doi:10.1002/2014JB011599.

Huang, W., van Hinsbergen, D.J.J., Dekkers, M.J., Garzanti, E., Dupont-Nivet, G., Lippert, P.C., Li, X., Maffione, M., Langereis, C.G., Hu, X., Guo, Z., and Kapp, P., 2015b, Paleolatitudes of the Tibetan Himalaya from primary and secondary magnetizations of Jurassic to Lower Cretaceous sedimentary rocks: Geochemistry Geophysics Geosystems, v. 16, p. 77–100, doi:10.1002/2014GC005624.

Jones, C.H., 2002, User-driven integrated software lives: "Paleomag" paleomagnetics analysis on the Macintosh: Computers & Geosciences, v. 28, p. 1145–1151, doi:10.1016/S0098-3004(02)00032-8.

Kent, D.V., 1985, Thermoviscous remagnetization in some Appalachian limestones: Geophysical Research Letters, v. 12, p. 805–808, doi:10.1029/GL012i012p00805.

Kent, D.V., Zeng, X.S., Zhang, W.Y., and Opdyke, N.D., 1987, Widespread late Mesozoic to recent remagnetization of Paleozoic and Lower Triassic sedimentary rocks from South China: Tectonophysics, v. 139, p. 133–143, doi:10.1016/0040-1951(87)90202-2.

Kirschvink, J., 1980, The least-squares line and plane and the analysis of palaeomagnetic data: Geophysical Journal International, v. 62, p. 699–718, doi:10.1111/j.1365-246X.1980.tb02601.x.

Kondo, K., Mu, C.L., Yamamoto, T., Zaman, H., Miura, D., Yokoyama, M., Ahn, H.S., and Otofuji, Y., 2012, Oroclinal origin of the Simao arc in the Shan-Thai block inferred from the Cretaceous palaeomagnetic data: Geophysical Journal International, v. 190, no. 1, p. 201–216, doi:10.1111/j.1365-246X.2012.05467.x.

Kornfeld, D., Eckert, S., Appel, E., Ratschbacher, L., Pfander, J., Liu, D., and Ding, L., 2014a, Clockwise rotation of the Baoshan block due to southeastward tectonic escape of Tibetan crust since the Oligocene: Geophysical Journal International, v. 197, p. 149–163, doi:10.1093/gji/ggu009.

Kornfeld, D., Eckert, S., Appel, E., Ratschbacher, L., Sonntag, B.L., Pfänder, J.A., Ding, L., and Liu, D., 2014b, Cenozoic clockwise rotation of the Tengchong block, southeastern Tibetan Plateau: A paleomagnetic and geochronologic study: Tectonophysics, v. 628, p. 105–122, doi:10.1016/j.tecto.2014.04.032.

Koymans, M.R., Langereis, C.G., Pastor-Galan, D., and van Hinsbergen, D.J.J., 2016, Paleomagnetism.org: An online multi-platform open source environment for paleomagnetic data analysis: Computers & Geosciences, v. 93, p. 127–137, doi:10.1016/j.cageo.2016.05.007.

Kruiver, P., Dekkers, M.J., and Heslop, D., 2001, Quantification of magnetic coercivity components by the analysis of acquisition curves of isothermal remanent magnetisation: Earth and Planetary Science Letters, v. 189, no. 3–4, p. 269–276, doi:10.1016/S0012-821X(01)00367-3.

Leloup, P., Lacassin, R., Tapponnier, P., Scharer, U., Zhong, D.L., Liu, X.H., Zhang, L.S., Ji, S.C., and Trinh, P.T., 1995, The Ailao Shan–Red River shear zone (Yunnan, China), Tertiary transform boundary of Indochina: Tectonophysics, v. 251, no. 1–4, p. 3–84, doi:10.1016/0040-1951(95)00070-4.

Leloup, P.H., Arnaud, N., Lacassin, R., Kienast, J.R., Harrison, T.M., Trong, T.T.P., Replumaz, A., and Tapponnier, P., 2001, New constraints on the structure, thermochronology, and timing of the Ailao Shan–Red River shear zone, SE Asia: Journal of Geophysical Research, v. 106, no. B4, p. 6683–6732, doi:10.1029/2000JB900322.

Li, S.H., Huang, B.C., and Zhu, R.X., 2012, Palaeomagnetic constraints on the tectonic rotation of the southeastern margin of the Tibetan Plateau: Chinese Journal of Geophysics, v. 55, p. 76–94, doi:10.1002/cjg2.1702.

Li, S.H., Deng, C.L., Yao, H.T., Huang, S., Liu, C.Y., He, H.Y., Pan, Y.X., and Zhu, R.X., 2013, Magnetostratigraphy of the Dali Basin in Yunnan and implications for late Neogene rotation of the southeast margin of the Tibetan Plateau: Journal of Geophysical Research, v. 118, p. 791–808, doi:10.1002/jgrb.50129.

Li, S.H., Deng, C.L., Dong, W., Sun, L., Liu, S.Z., Qin, H.F., Yin, J.Y., Ji, X.P., and Zhu, R.X., 2015, Magnetostratigraphy of the Xiaolongtan Formation bearing *Lufengpithecus keiyuanensis* in Yunnan, southwestern China: Constraint on the initiation time of the southern segment of the Xianshuihe-Xiaojiang fault: Tectonophysics, v. 655, p. 213–226, doi:10.1016/j.tecto.2015.06.002.

Li, Y.X., and Kodama, K.P., 2016, Detecting and correcting for paleomagnetic inclination shallowing of sedimentary rocks: A review: Frontiers of Earth Science, v. 4, no. 7, doi:10.3389/feart.2016.00007.

Lippert, P., van Hinsbergen, D., and Dupont-Nivet, G., 2014, Early Cretaceous to present latitude of the central proto–Tibetan Plateau: A paleomagnetic synthesis with implications for Cenozoic tectonics, paleogeography, and climate of Asia, *in* Nie, J., Hoke, G.D., and Horton, B.K., eds., Toward an Improved Understanding of Uplift Mechanisms and the Elevation History of the Tibetan Plateau: Geological Society of America Special Paper 507, p. 1–21, doi:10.1130/2014.2507(01).

Liu, C.Y., Ge, K.P., Zhang, C.X., Liu, Q.S., Deng, C.L., and Zhu, R.X., 2011, Nature of remagnetization of Lower Triassic red beds in southwestern China: Geophysical Journal International, v. 187, p. 1237–1249, doi:10.1111/j.1365-246X.2011.05196.x.

Lowrie, W., 1990, Identification of ferromagnetic minerals in a rock by coercivity and unblocking temperature properties: Geophysical Research Letters, v. 17, no. 2, p. 159–162, doi:10.1029/GL017i002p00159.

McCabe, C., and Elmore, R.D., 1989, The occurrence and origin of late Paleozoic remagnetization in the sedimentary rocks of North America: Reviews of Geophysics, v. 27, p. 471–494, doi:10.1029/RG027i004p00471.

McElhinny, M., 1964, Statistical significance of the fold test in paleomagnetism: Geophysical Journal of the Royal Astronomical Society, v. 8, p. 338–340, doi:10.1111/j.1365-246X.1964.tb06300.x.

McFadden, P., 1990, A new fold test for paleomagnetic studies: Geophysical Journal International, v. 103, p. 163–169, doi:10.1111/j.1365-246X.1990.tb01761.x.

McFadden, P., and McElhinny, M., 1990, Classification of the reversal test in paleomagnetism: Geophysical Journal International, v. 103, no. 3, p. 725–729.

Molnar, P., and Tapponnier, P., 1975, Cenozoic tectonics of Asia: Effects of a continental collision: Features of recent continental tectonics in Asia can be interpreted as results of the India-Eurasia collision: Science, v. 189, p. 419–426, doi:10.1126/science.189.4201.419.

Ogg, J.G., 2012, Geomagnetic polarity time scale, *in* Gradstein, F.M., Ogg, J.G., Schmitz, M.D., and Ogg, G.M., eds., The Geologic Time Scale 2012: Amsterdam, Netherlands, Elsevier BV, p. 85–113, doi:10.1016/B978-0-444-59425-9.00005-6.

Otofuji, Y., Inoue, Y., Funahara, S., Murata, F., and Zheng, X., 1990, Paleomagnetic study of eastern Tibet: Deformation of the Three Rivers region: Geophysical Journal International, v. 103, p. 85–94, doi:10.1111/j.1365-246X.1990.tb01754.x.

Otofuji, Y., Yokoyama, M., Kitada, K., and Zaman, H., 2010, Paleomagnetic versus GPS determined tectonic rotation around eastern Himalayan syntaxis in East Asia: Journal of Asian Earth Sciences, v. 37, p. 438–451, doi:10.1016/j.jseaes.2009.11.003.

Otofuji, Y., Tung, V.D., Fujihara, M., Tanaka, M., Yokoyama, M., Kitada, K., and Zaman, H., 2012, Tectonic deformation of the southeastern tip of the Indochina Peninsula during its southward displacement in the Cenozoic time: Gondwana Research, v. 22, no. 2, p. 615–627, doi:10.1016/j.gr.2011.09.015.

Roger, F., Calassou, S., Lancelot, J., Malavieille, J., Mattauer, M., Xu, Z.Q., Hao, Z.W., and Hou, L.W., 1995, Miocene emplacement and deformation of the Konga-Shan Granite (Xianshui-He fault zone, west Sichuan, China)—Geodynamic implications: Earth and Planetary Science Letters, v. 130, no. 1–4, p. 201–216, doi:10.1016/0012-821X(94)00252-T.

Royden, L.H., Burchfiel, B.C., and van der Hilst, R.D., 2008, The geological evolution of the Tibetan Plateau: Science, v. 321, p. 1054–1058, doi:10.1126/science.1155371.

Sato, K., Liu, Y., Zhu, Z., Yang, Z., and Otofuji, Y.-I., 1999, Paleomagnetic study of middle Cretaceous rocks from Yunlong, western Yunnan, China: Evidence of southward displacement of Indochina: Earth and Planetary Science Letters, v. 165, no. 1, p. 1–15, doi:10.1016/S0012-821X(98)00257-X.

Sato, K., Liu, Y.Y., Zhu, Z.C., Yang, Z.Y., and Otofuji, Y., 2001, Tertiary paleomagnetic data from northwestern Yunnan, China: Further evidence for large clockwise rotation of the Indochina block and its tectonic implications: Earth and Planetary Science Letters, v. 185, no. 1–2, p. 185–198, doi:10.1016/S0012-821X(00)00377-0.

Sato, K., Liu, Y.Y., Wang, Y.B., Yokoyama, M., Yoshioka, S., Yang, Z., and Otofuji, Y.I., 2007, Paleomagnetic study of Cretaceous rocks from Pu'er, western Yunnan, China: Evidence of internal deformation of the Indochina block: Earth and Planetary Science Letters, v. 258, p. 1–15, doi:10.1016/j.epsl.2007.02.043.

Schoenbohm, L.M., Burchfiel, B.C., Chen, L.Z., and Yin, J.Y., 2005, Exhumation of the Ailao Shan shear zone recorded by Cenozoic sedimentary rocks, Yunnan Province, China: Tectonics, v. 24, TC6015, doi:10.1029/2005TC001803.

Schoenbohm, L., Burchfiel, B.C., Chen, L., and Yin, J., 2006, Miocene to present activity along the Red River fault, China, in the context of continental extrusion, upper-crustal rotation, and lower-crustal flow: Geological Society of America Bulletin, v. 118, no. 5–6, p. 672–688, doi:10.1130/B25816.1.

Searle, M., Yeh, M.W., Lin, T.H., and Chung, S.L., 2010, Structural constraints on the timing of left-lateral shear along the Red River shear zone in the Ailao Shan and Diancang Shan Ranges, Yunnan, SW China: Geosphere, v. 6, no. 4, p. 316–338, doi:10.1130/GES00580.1.

Singsoupho, S., Bhongsuwan, T., and Elming, S.-Å., 2014, Tectonic evaluation of the Indochina block during Jurassic–Cretaceous from palaeomagnetic results of Mesozoic redbeds in central and southern Lao PDR: Journal of Asian Earth Sciences, v. 92, p. 18–35, doi:10.1016/j.jseaes.2014.06.001.

Spurlin, M.S., Yin, A., Horton, B.K., Zhou, J., and Wang, J., 2005, Structural evolution of the Yushu-Nangqian region and its relationship to syncollisional igneous activity east-central Tibet: Geological Society of America Bulletin, v. 117, no. 9–10, p. 1293–1317, doi:10.1130/B25572.1.

Takemoto, K., Halim, N., Otofuji, Y., Van Tri, T., Van De, L., and Hada, S., 2005, New paleomagnetic constraints on the extrusion of Indochina: Late Cretaceous results from the Song Da terrane, northern Vietnam: Earth and Planetary Science Letters, v. 229, no. 3–4, p. 273–285, doi:10.1016/j.epsl.2004.09.040.

Takemoto, K., Sato, S., Chanthavichith, K., Inthavong, T., Inokuchi, H., Fujihara, M., Zaman, H., Yang, Z., Yokoyama, M., Iwamoto, H., and Otofuji, Y.-I., 2009, Tectonic deformation of the Indochina Peninsula recorded in the Mesozoic palaeomagnetic results: Geophysical Journal International, v. 179, no. 1, p. 97–111, doi:10.1111/j.1365-246X.2009.04274.x.

Tan, X., 1999, Characteristics and formation mechanism of Cenozoic structural basins in the Three-River area of west Yunnan: Yunnan Geology, v. 18, no. 2, p. 112–121.

Tanaka, K., Mu, C., Sato, K., Takemoto, K., Miura, D., Liu, Y., Zaman, H., Yang, Z., Yokoyama, M., Iwamoto, H., Uno, K., and Otofuji, Y.-I., 2008, Tectonic deformation around the eastern Himalayan syntaxis: Constraints from the Cretaceous palaeomagnetic data of the Shan-Thai block: Geophysical Journal International, v. 175, no. 2, p. 713–728, doi:10.1111/j.1365-246X.2008.03885.x.

Tapponnier, P., Peltzer, G., Le Dain, A.Y., Armijo, R., and Cobbold, P., 1982, Propagating extrusion tectonics in Asia: New insights from simple experiments with plasticine: Geology, v. 10, p. 611–616, doi:10.1130/0091-7613(1982)10<611:PETIAN>2.0.CO;2.

Tauxe, L., 2010, Essentials of Paleomagnetism: Berkeley, California, University of California Press, 512 p.

Tauxe, L., and Kent, D.V., 2004, A simplified statistical model for the geomagnetic field and the detection of shallow bias in paleomagnetic inclinations: Was the ancient magnetic field dipolar?, *in* Channell, J.E.T., Kent, D.V., Lowrie, W., and Meert, J.G., eds., Timescales of the Paleomagnetic Field: American Geophysical Union Geophysical Monograph 145, p. 101–115, doi:10.1029/145GM08.

Tauxe, L., and Watson, G.S., 1994, The fold test: An eigen analysis approach: Earth and Planetary Science Letters, v. 122, p. 331–341, doi:10.1016/0012-821X(94)90006-X.

Tauxe, L., Kodama, K.P., and Kent, D.V., 2008, Testing corrections for paleomagnetic inclination error in sedimentary rocks: A comparative approach: Physics of the Earth and Planetary Interiors, v. 169, no. 1–4, p. 152–165, doi:10.1016/j.pepi.2008.05.006.

Tong, Y.B., Yang, Z., Zheng, L.D., Xu, Y.L., Wang, H., Gao, L., and Hu, X.Z., 2013, Internal crustal deformation in the northern part of Shan-Thai block: New evidence

from paleomagnetic results of Cretaceous and Paleogene redbeds: Tectonophysics, v. 608, p. 1138–1158, doi:10.1016/j.tecto.2013.06.031.

Tong, Y.B., Yang, Z., Wang, H., Gao, L., An, C.Z., Zhang, X.D., and Xu, Y.C., 2015, The Cenozoic rotational extrusion of the Chuan Dian fragment: New paleomagnetic results from Paleogene red-beds on the southeastern edge of the Tibetan Plateau: Tectonophysics, v. 658, p. 46–60, doi:10.1016/j.tecto.2015.07.007.

Tong, Y.B., Yang, Z., Jing, X., Zhao, Y., Li, C., Huang, D., and Zhang, X., 2016, New insights into the Cenozoic lateral extrusion of crustal blocks on the southeastern edge of Tibetan Plateau: Evidence from paleomagnetic results from Paleogene sedimentary strata of the Baoshan terrane: Tectonics, v. 35, p. 2494–2514, doi:10.1002/2016TC004221.

Torsvik, T.H., Van der Voo, R., Preeden, U., MacNiocaill, C., Steinberger, B., Doubrovine, P.V., van Hinsbergen, D.J.J., Domeier, M., Gaina, C., Tohver, E., Meert, J.G., McCausland, P.J.A., and Cocks, L.R.M., 2012, Phanerozoic polar wander, palaeogeography and dynamics: Earth-Science Reviews, v. 114, p. 325–368, doi:10.1016/j.earscirev.2012.06.007.

Tsuchiyama, Y., Zaman, H., Sotham, S., Samuth, Y., Sato, E., Ahn, H.S., Uno, K., Tsumura, K., Miki, M., and Otofuji, Y.I., 2016, Paleomagnetism of Late Jurassic to Early Cretaceous red beds from the Cardamom Mountains, southwestern Cambodia: Tectonic deformation of the Indochina Peninsula: Earth and Planetary Science Letters, v. 434, p. 274–288, doi:10.1016/j.epsl.2015.11.045.

van Hinsbergen, D.J.J., Steinberger, B., Doubrovine, P.V., and Gassmöller, R., 2011a, Acceleration and deceleration of India-Asia convergence since the Cretaceous: Roles of mantle plumes and continental collision: Journal of Geophysical Research, v. 116, B06101, doi:10.1029/2010JB008051.

van Hinsbergen, D.J.J., Kapp, P., Dupont-Nivet, G., Lippert, P.C., DeCelles, P.G., and Torsvik, T.H., 2011b, Restoration of Cenozoic deformation in Asia and the size of Greater India: Tectonics, v. 30, TC5003, doi:10.1029/2011TC002908.

van Hinsbergen, D.J., Lippert, P.C., Dupont-Nivet, G., McQuarrie, N., Doubrovine, P.V., Spakman, W., and Torsvik, T.H., 2012, Greater India Basin hypothesis and a two-stage Cenozoic collision between India and Asia: Proceedings of the National Academy of Sciences of the United States of America, v. 109, no. 20, p. 7659–7664, doi:10.1073/pnas.1117262109.

Wang, E., Burchfiel, B.C., Royden, L.H., Chen, L.Z., Chen, J.S., Li, W.X., and Chen, Z.L., 1998, Late Cenozoic Xianshuihe-Xiaojiang, Red River, and Dali Fault Systems of Southwestern Sichuan and Central Yunnan, China: Geological Society of America Special Paper 327, 108 p.

Wang, E., Kirby, E., Furlong, K.P., van Soest, M., Xu, G., Shi, X., Kamp, P.J.J., and Hodges, K.V., 2012, Two-phase growth of high topography in eastern Tibet during the Cenozoic: Nature Geoscience, v. 5, no. 9, p. 640–645, doi:10.1038/ngeo1538.

Wang, L., Liu, C., Fei, M., Shen, L., Zhang, H., and Zhao, Y., 2015, First SHRIMP U-Pb zircon ages of the potash-bearing Mengyejing Formation, Simao Basin, southwestern Yunnan, China: Cretaceous Research, v. 52, p. 238–250, doi:10.1016/j.cretres.2014.09.008.

Wang, S., Fang, X.M., Zheng, D.W., and Wang, E.C., 2009, Initiation of slip along the Xianshuihe fault zone, eastern Tibet, constrained by K/Ar and fission-track ages: International Geology Review, v. 51, no. 12, p. 1121–1131, doi:10.1080/00206810902945132.

Wang, W.M., 1996, A palynological survey of Neogene strata in Xiaolongtan Basin, Yunnan Province of South China: Acta Botanica Sinica, v. 38, no. 9, p. 743–748.

Xu, W., Xia, G., An, Z., Chen, G., Zhang, F., Wang, Y., Tian, Y., Wei, Z., Ma, S., and Chen, H., 2003, Magnetic survey and ChinaGRF 2000: Earth Planets Spaces, v. 55, p. 215–217.

Yamashita, I., Surinkum, A., Wada, Y., Fujihara, M., Yokoyama, M., Zaman, H., and Otofuji, Y.I., 2011, Paleomagnetism of the Middle-Late Jurassic to Cretaceous red beds from the Peninsular Thailand: Implications for collision tectonics: Journal of Asian Earth Sciences, v. 40, p. 784–796, doi:10.1016/j.jseaes.2010.11.001.

Yang, T.N., Liang, M.J., Fan, J.W., Shi, P.L., Zhang, H.R., and Hou, Z.H., 2014, Paleogene sedimentation, volcanism, and deformation in eastern Tibet: Evidence from structures, geochemistry, and zircon U-Pb dating in the Jianchuan Basin, SW China: Gondwana Research, v. 26, no. 2, p. 521–535, doi:10.1016/j.gr.2013.07.014.

Yang, Z.Y., and Besse, J., 1993, Paleomagnetic study of Permian and Mesozoic sedimentary rocks from northern Thailand supports the extrusion model for Indochina: Earth and Planetary Science Letters, v. 117, p. 525–552, doi:10.1016/0012-821X(93)90101-E.

Yang, Z.Y., and Otofuji, Y., 2001, Paleomagnetic study of the Early Tertiary on both sides of the Red River fault and its geological implications: Acta Geologica Sinica, v. 75, no. 1, p. 35–44.

Yang, Z.Y., Besse, J., Sutheetorn, V., Bassoullet, J.P., Fontaine, H., and Buffetaut, E., 1995, Lower-Middle Jurassic paleomagnetic data from the Mae Sot area (Thailand): Paleogeographic evolution and deformation history of southeastern Asia: Earth and Planetary Science Letters, v. 136, p. 325–341, doi:10.1016/0012-821X(95)00192-F.

Yang, Z.Y., Yin, J.Y., Sun, Z.M., Otofuji, Y., and Sato, K., 2001, Discrepant Cretaceous paleomagnetic poles between eastern China and Indochina: A consequence of the extrusion of Indochina: Tectonophysics, v. 334, p. 101–113, doi:10.1016/S0040-1951(01)00061-0.

Yi, Z., Huang, B.C., Chen, J.S., Chen, L.W., and Wang, H.L., 2011, Paleomagnetism of early Paleogene marine sediments in southern Tibet, China: Implications to onset of the India-Asia collision and size of Greater India: Earth and Planetary Science Letters, v. 309, p. 153–165, doi:10.1016/j.epsl.2011.07.001.

Yunnan Bureau of Geology and Mineral Resources (YBGMR), 1990, Regional Geology of Yunnan Province: Beijing, Geological Publishing House, 726 p. [in Chinese].

Zhou, J.Y., Wang, J.H., Horton, B.K., Yin, A., and Spurlin, M.S., 2007, Sedimentology and chronology of Paleogene coarse clastic rocks in east-central Tibet and their relationship to early tectonic uplift: Acta Geological Sinica–English Edition, v. 81, p. 398–408, doi:10.1111/j.1755-6724.2007.tb00963.x.

Zhu, R., Potts, R., Pan, Y.X., Lue, L.Q., Yao, H.T., Deng, C.L., and Qin, H.F., 2008, Paleomagnetism of the Yuanmou Basin near the southeastern margin of the Tibetan Plateau and its constraints on late Neogene sedimentation and tectonic rotation: Earth and Planetary Science Letters, v. 272, no. 1–2, p. 97–104, doi:10.1016/j.epsl.2008.04.016.

Zijderveld, J., 1967, AC demagnetization of rocks: Analysis of results, *in* Collinson, D.W., Creer, K.M., and Runcorn, S.K., eds., Methods in Paleomagnetism: Amsterdam, Netherlands, Elsevier, p. 254–286.

Science Editor: Bradley S. Singer
Associate Editor: Massimo Mattei

Manuscript Received 23 August 2016
Revised Manuscript Received 11 February 2017
Manuscript Accepted 20 March 2017

Printed in the USA